12-2015

Studying the Optimum Design of Automotive Thermoelectric Air Conditioning

Alaa Attar
Western Michigan University, alaa_attar@yahoo.com

STUDYING THE OPTIMUM DESIGN OF AUTOMOTIVE THERMOELECTRIC AIR CONDITIONING

by

Alaa Attar

A dissertation submitted to the Graduate College
in partial fulfillment of the requirements
for the degree of Doctoral of Philosophy
Mechanical and Aerospace Engineering
Western Michigan University
December 2015

Doctoral Committee:

HoSung Lee, Ph.D., Chair
Chris Cho, Ph.D.
Muralidhar Ghantasala, Ph.D.
John Cameron, Ph.D.

STUDYING THE OPTIMUM DESIGN OF AUTOMOTIVE THERMOELECTRIC AIR CONDITIONING

Alaa Attar, Ph.D.

Western Michigan University, 2015

The remarkable amount of research being conducted on thermoelectrics gives the impression that this technology will have a bright future in power generation and temperature control systems. At the present time, thermoelectrics is applied widely for temperature control, but has not yet replaced conventional air-conditioning systems due to its lower performance. Currently, approximately 10% of annual vehicle fuel consumption corresponds to the air-conditioning system used to cool the vehicle cabin. Conventional air-conditioning systems cool the entire cabin; however, about 73% of a vehicle's mileage occurs while the driver is the only occupant. These facts indicate the need for a single occupant zone air-conditioning system. Thermoelectrics is one of the best technologies to meet this need because it is a very scalable system, wherein a miniature air-conditioning system can be built using a thermoelectric cooler.

The current project discusses the optimization of a counter flow air-to-air thermoelectric air conditioner (TEAC) system. The work utilizes a newly developed optimal design theory and dimensional analysis technique, which allows for optimization of thermoelectric parameters simultaneously. Applying this method on a unit cell located at the center of the TEAC system provides a simple way to study the optimum design and its feasibility; however, further studies are needed to simulate the optimum design of an

entire TEAC system from given inlet parameters (i.e., hot and cold air mass flow rates and ambient temperatures). The analytical model, therefore, is built by combining optimal design and thermal isolation methods so that the thermoelectric parameters of the whole system can be simulated and optimized. Based on the designed models, two experiments (one for the unit cell and the other for the whole system) are conducted in order to study the accuracy of the analytical models. Although the analytical model was built based on thermoelectric ideal equations, the results show good agreements with the experiments. These agreements are mainly due to the use of thermoelectric effective material properties, which are obtained from the measured maximum thermoelectric module parameters. The validation of the analytical model provides an uncomplicated method to study the optimum design at given inputs.

ACKNOWLEDGEMENTS

I would like to specially thank my advisor, Dr. HoSung Lee, for his encouragement and patience. The completion of this dissertation would not have been possible without his constant direction and motivation. I'm very lucky and thankful to have someone like Dr. Lee who always dedicates himself to educate his students.

I would also like to extend my thanks to my committee members Dr. Chris Cho, Dr. Muralidhar Ghantasala, and Dr. John Cameron for their guidance and helpful suggestions to improve the quality of this work.

I wish to thank the government of Saudi Arabia who believed in me and provided me with a generous scholarship.

I would also like to thank my entire family, especially my mother, my wife, and my children for all of their support and sacrifices that are a big part of my accomplishment and I'm always grateful to be surrounded by them. Their love and support are the sources that provide me with the energy and courage. Also, all the support I had from all my friends and extended family is much appreciated.

Alaa Attar

TABLE OF CONTENTS

Table of Contents—Continued

CHAPTER

Table of Contents—Continued

CHAPTER

LIST OF TABLES

LIST OF FIGURES

List of Figures—Continued

List of Figures—Continued

NOMENCLATURE

A_c	total fin surface area cold side heat sink (mm^2)
A_e	cross-sectional area of thermoelement (mm^2)
A_h	total fin surface area hot side heat sink (mm^2)
A_M	base area of thermoelectric module (mm^2)
COP	the coefficient of performance
c_p	specific heat (J/kg.K)
G_e	thermocouple geometric ratio
H	total height of thermoelectric air conditioner (mm)
h	heat transfer coefficient of the fluid (W/m^2K)
I	electric current (A)
j	unit cell number
L	total length of thermoelectric air conditioner (mm)
k	thermoelement thermal conductivity (W/m K), $k = k_p + k_n$
K	thermal conductance (W/K), $K = kA_e/L_e$
L_e	length of thermoelement (mm)
n	the number of thermocouples
N_k	dimensionless thermal conductance, $N_k = n(A_e k/L_e)/\eta_h h_h A_h$
N_h	dimensionless convection, $N_h = \eta_c h_c A_c/\eta_h h_h A_h$

N_I	dimensionless current, $N_I = \alpha I/(A_e k/L_e)$
P_{in}	input power (W)
q_x	the rate of heat transfer around the differential element
$\dot{Q}$	the rate of heat transfer
$\dot{Q}_c$	cooling capacity (W)
$\dot{Q}_h$	heat rejection (W)
R_{Al}	thermal resistance of the aluminum block
t_{al}	thickness of the aluminum block
T_c	cold junction temperature (°C)
T_h	hot junction temperature (°C)
$T_{\infty c}$	cold fluid temperature (°C)
$T_{\infty h}$	hot fluid temperature (°C)
$\dot{V}_c$	cold fluid volume flow rate (CFM)
$\dot{V}_h$	hot fluid volume flow rate (CFM)
W	total width of thermoelectric air conditioner (mm)
$\dot{W}$	electrical power (W)
x	direction along the length of the element
Z	the figure of merit (1/K) $= \alpha^2/\rho k$

Greek symbols

α	Seebeck coefficient (V/K), $\alpha = \alpha_p - \alpha_n$
ρ	electrical resistivity (Ω cm), $\rho = \rho_p + \rho_n$
φ	alimunum block thermal resistance (K/W)
η	fin efficiency of the heat sink
γ	thermal resistances ratio between the heat sink and aluminum block

Subscripts

al	aluminum
c	cold
ct	contact
e	thermoelement
h	hot
in	inlet
j	unit cell number
m	measured
n	n-type element
no	the number of thermocouples
out	outlet

opt.	optimal quantity
p	p-type element
$*$	dimensionless

CHAPTER 1

INTRODUCTION

The thermoelectric effect (abbreviated as TE) is the conversion of a difference in temperature to an electrical current, or vice versa. TE is used for several purposes including generating power, and heating and cooling. One of the benefits of TE is that it is a direct solid-state mechanism that does not require any fluid as an intermediate process, or contain any moving parts, which might increase the risk of the mechanical failure. As long as there is a temperature difference, thermoelectric devices are capable of generating power as presented in several applications. A thermoelectric generator (TEG), for example, was the source of power used for Curiosity, the rover sent to Mars in 2012. In the near future, TEGs may also be used to convert automobile exhaust waste heat into power, replacing the alternator [1]. Another thermoelectric device, the solar thermoelectric generator (STEG), captures and converts solar thermal energy to electricity for a variety of potential uses, including power plants and remote sensors. In its reversible process wherein electrical current is supplied to the thermoelectric device (known as TEC), TE can create the temperature difference that produces or pumps heat. TEC is seen in many applications such as mini refrigeration, microprocessor cooling, and medical applications.

1.1 Definition of Thermoelectrics and Thermoelectric Effects

In the early 19th century, Thomas Seebeck and Jean Peltier discovered and developed the concept of thermoelectricity. Thomas Seebeck discovered in 1821, that an electromotive force or a potential difference could be created by heating one side of a circuit made from a junction of two dissimilar wires. This electromotive force or the potential difference was named as the Seebeck effect. Thirteen years after Seebeck's discovery, Jean Peltier found out that the Seebeck effect is a reversible process. In other words, passing an electrical current through the circuit will heat one junction and will cool the other side of the junction. A thermoelectric module is formed when a number of dissimilar wires are connected thermally in parallel and electrically in series to each other. [2]

1.1.1 Seebeck Effect

The Seebeck effect is the conversion of a temperature difference on the two sides of the thermoelectric material into an electric current by creating free electrons and holes in the semiconductors. The movement of the electrons and the holes causes a current as shown in Figure 1.1 (a) and (b). If a voltmeter is placed between the semiconductor and the conductor, or between the cold side and the hot side, a potential difference will register on the voltmeter. This potential difference, which is the voltage V, is proportional to the temperature T. This relation can be summarized as follows. [2]

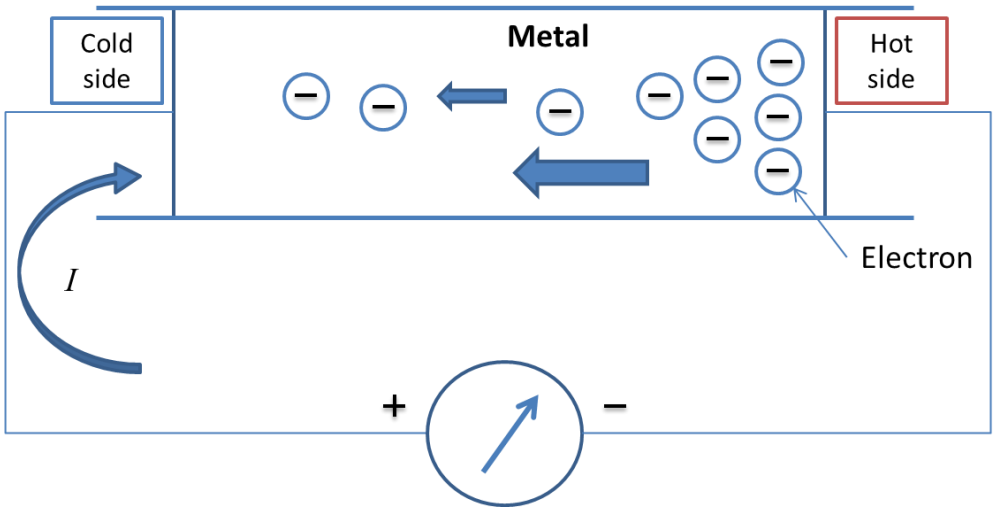

(a)

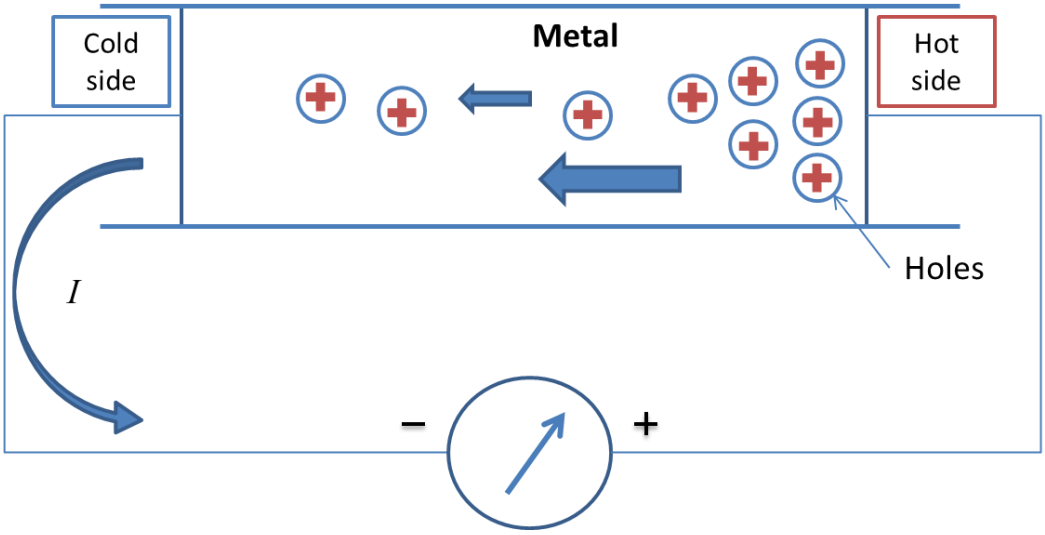

(b)

Figure 1.1 Seebeck effect and the movement of (a) electrons and (b) holes

$$V = \alpha \Delta T \qquad 1.1$$

ΔT is the temperature difference between either sides of the thermoelectric material and α is the Seebeck coefficient. ΔT and α are the two parameters which determine the voltage.

Depending on the resistance of the materials and the geometry, the amount of current can be determined. [2]

1.1.2 Peltier Effect

When current is passing across a junction between two conductors, heat must be continuously supplemented or deducted at the junction to keep the junction temperature constant. The amount of heat being moved across the junction is proportional to the current. The Peltier effect can be represented by the following equation

$$Q_{peltier} = \pi_{AB} I \qquad 1.2$$

where $Q_{peltier}$ represents the heat absorbed or liberated, I is the current passing though the thermoelectric material, and π_{AB} is the Peltier coefficient. [2]

1.1.3 Thomson Effect

The Thomson effect is similar to the Peltier effect in many ways, but the main difference is that Thomson effect needs a temperature gradient and a flowing current. When the current flows through a wire with a temperature gradient, heat will be absorbed or liberated across the wire depending on the material and current direction. Heat absorption or liberation is proportional to the current and the temperature gradient. The Thomson heat transfer rate $Q_{Thomson}$ is defined by the equation

$$Q_{Thomson} = \tau \Delta T \, I \qquad 1.3$$

where τ is the Thomson coefficient. [2]

1.1.4 The Figure of Merit

The figure of merit, Z, is a method used to measure the performance of a thermoelectric device where it is equal to

$$Z = \frac{\alpha^2}{\rho k} \tag{1.4}$$

where ρ is the electrical resistivity in Ohm-m and k is the thermal conductivity in W/mK.

A higher Z can result from higher α and/or lower ρ and k. These parameters depend on the type of material at a given temperature where it can be shown as dimensionless number ZT. Therefore, in order to have a higher TE performance, a material with higher ZT value should be used. Bismuth Telluride (Bi_2Te_3) is one of the most widely used bulk materials for thermoelectric cooler (TEC) applications due to its high figure of merit at room temperature. Other bulk materials such as Lead Telluride (PbTe) are also found in TE modules especially for higher temperature and thermoelectric generators (TEG) applications. [2]

With the aim of obtaining higher ZT values, nano-materials have been investigated where ZT can be higher than one. The use of nanotechnology is to either increase the power factor which is the Seebeck coefficient and electrical conductivity ($1/\rho$), or to decrease the thermal conductivity which consists of electronic and lattice thermal conductivities. The Seebeck coefficient and electrical conductivity are usually related inversely, which makes it more complicated to increase any of them. Moreover, decreasing the thermal conductivity will increase the electrical conductivity due to the constant relationship between the electrical conductivity and electronic thermal conductivity, i.e., the Lorentz number [3]. Hence, the lattice thermal conductivity, which

is the only parameter that is almost independent of the electronic structure, can be reduced by manipulating the phonon scattering [3]. Figure 1.2 presents state-of-the-art of the dimensionless figure of merit of the old and new thermoelectric material [4]. It can be seen from the figure that bismuth telluride has the highest figure of merit for bulk material at room temperature. Also, nano-material shows a noticeable improvement that provides a higher figure of merit.

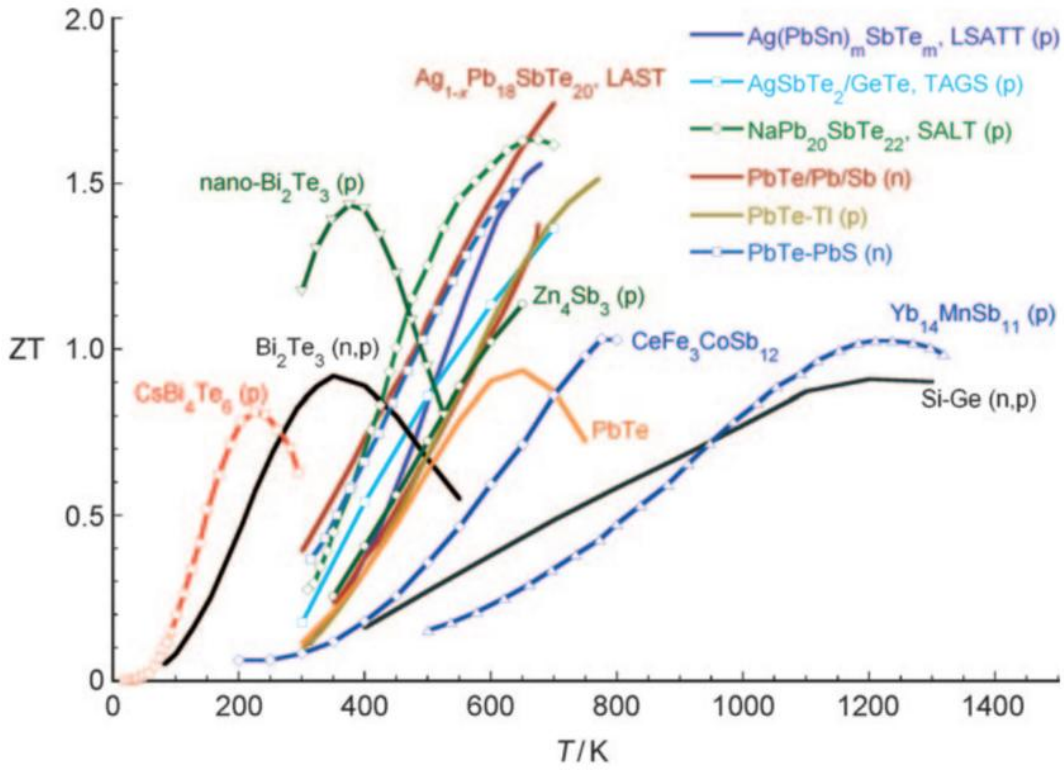

Figure 1.2 Plot of state-of-the-art of the figure of merit vs. temperature of thermoelectric materials. [4]

1.2 Automotive Thermoelectric Air Conditioners (TEAC)

1.2.1 Background

As shown in the examples discussed earlier, the concept of thermoelectrics is growing in its use and applications. Automotive thermoelectric air conditioners are one in particular of the newer applications. Approximately 10% of annual vehicle fuel consumption corresponds to the air-conditioning (AC) system used to cool the vehicle cabin. Most of these ACs use refrigerant R-134a, which does not have the ozone-depleting properties of Freon, but is nevertheless a terrible greenhouse gas [5]. It is likely that R-134a will be banned in the near future, which means the automotive industry needs an alternative AC technology [5]. In 2009, the U.S. Department of Energy (DOE) and the California Energy Commission funded a project to research the use of a thermoelectric heating ventilation and air conditioner (TE HVAC) systems to replace existing conventional AC systems in automobiles [6]. Use of a thermoelectric air conditioning (TEAC) system instead of a conventional AC system was found to have the benefits of eliminating the need for R-134a, as well as the ability to pump the heat from selected zones instead of the entire cabin, which, in turn, reduces fuel consumption [4]. TEAC systems do appear to be, in fact, a promising alternative to conventional AC systems.

A primary goal of the DOE project was to design a TEAC system that could provide the cooling power for a single occupant with at least 1.3 of coefficient of performance (COP) [7]. About 73% of a vehicle's mileage occurs when the driver is the only occupant, which requires only 630W to cool his or her occupant zone and 3.5 to 4.5 kW to cool the entire cabin [6].

Table 1.1 shows Schlesinger's [8] comparison between TEAC and conventional air-conditioning systems. As shown, the thermoelectric cooler has several advantages over the compressor cooler.

Table 1.1

The Comparison Between Thermoelectric Air Conditioning and Traditional Compressor System [5]

Comparing factor	**Thermoelectric cooler**	**Compressor Cooler**
Size	Small	Big
Weight	5kg to 8kg	10kg to 15kg
Accessories/ pipeline	Less	More
Environmental protection	No refrigerant	Need refrigerants
Orientation	No limit	With limit
Moving Parts	No moving parts	With moving parts
Reliability	> 100,000 hr	< 40,000 hr

1.2.2 Current State in Automotive TEAC

Several designs of automotive air-to-liquid TEAC systems are shown in the literature, and will be discussed in the literature review section of this dissertation. In general, a close analysis of individual performance shows that none of these designs is the optimum TEAC system. Nevertheless, a design presented by the Ford Motor Company in collaboration with Gentherm stands out due to its superior performance. This design was funded by the DOE in the latter's efforts to create a zonal auto TEAC system [6]. Gentherm offered a proposal with a feasible air-to-liquid TEAC that met the requirements of the DOE [9]. It shows more applicability because of its higher power density when compared with other air-to-liquid TEAC systems.

Finding the optimum design of a thermoelectric system is a challenging task due to the inescapable need to simultaneously optimize several parameters. Recently, Lee [10] developed a new optimum design method that allows thermoelectric parameters to be optimized simultaneously by using a dimensional analysis technique. The present work implements the optimal design method on the Gentherm air-to-liquid TEAC design and studies the possibility of any improvement in *COP*. This improvement, if any, could result from optimizing the electrical current and the thermoelectric geometric ratio (or number of thermoelectric thermocouples). There is a question as to whether the same theory could be applied when assessing the performance of an air-to-air TEAC system and meeting the DOE requirements ($Q_c = 630W$ & $COP = 1.3$).

When using the optimum design method, two technical obstructions have to be addressed. First, the optimum design method works with constant ambient temperatures. However, the nature of the temperature of previously studied TEAC systems is bound to change along with the length of the system. This obstruction could be resolved by applying the thermal isolation method [11]. Second, the optimal design method uses the thermoelectric ideal equations, which does not include the effects of contact resistance. This may be corrected by using the *effective material properties*, which can be calculated from the experimentally obtained maximum parameters of a commercial thermoelectric module [12].

Optimal designs are analytical approaches that need to be validated with experiments. In particular, constructing and testing an optimized air-to-air TEAC system is necessary to show the accuracy of the theoretical design when compared to a realistic design. Based on the optimum design of a unit cell, an experiment can validate the

accuracy of the analytical design. On the other hand, the optimal design method can be combined with the thermal isolation method in order to optimize a TEAC's entire system. This goal may be reached by simulating four unit cells wherein these unit cells are located at the intersection of two planes of symmetry, which also needs to be experimentally validated.

CHAPTER 2

BACKGROUND OF THERMOELECTRICS

Before studying the optimum design of the automotive thermoelectric air conditioner, the basic concepts of thermoelectrics needs be discussed. Therefore, the main purpose of this chapter is to summarize all related background information about thermoelectrics that assist with understanding the related aspects of the current research. These concepts are mostly adopted from Ref. [2] in addition to some modifications and studies addressed and cited from other resources as needed.

2.1 Thermoelectric Module Ideal Equations

As discussed in Chapter 1, a voltage can be created by heating one side of a circuit made from a junction of two dissimilar semiconductors. Therefore, the heat absorbed or released at the junctions of the semiconductors will consist of the Peltier cooling in addition to Joule heating (resulted from the flow of the electrical current) and thermal conduction. Consequently, this section focuses on how the thermoelectrics equations are formulated in addition to addressing the performances of the thermoelectric modules.

2.1.1 Equations Formulations [2]

Given are two dissimilar semiconductors which are connected thermally in parallel and electrically in series where the heat is supplied from one side (side 1) and

released from the other (side 2). Each semiconductor has a temperature independent Seebeck coefficient (α), electrical resistivity (ρ), and thermal conductivity (k). Figure 2.1 (a) shows a thermoelectric couple that consists of p-type material (positive) and n-type material (negative). The steady state heat balance at junction 1 at T_1 becomes

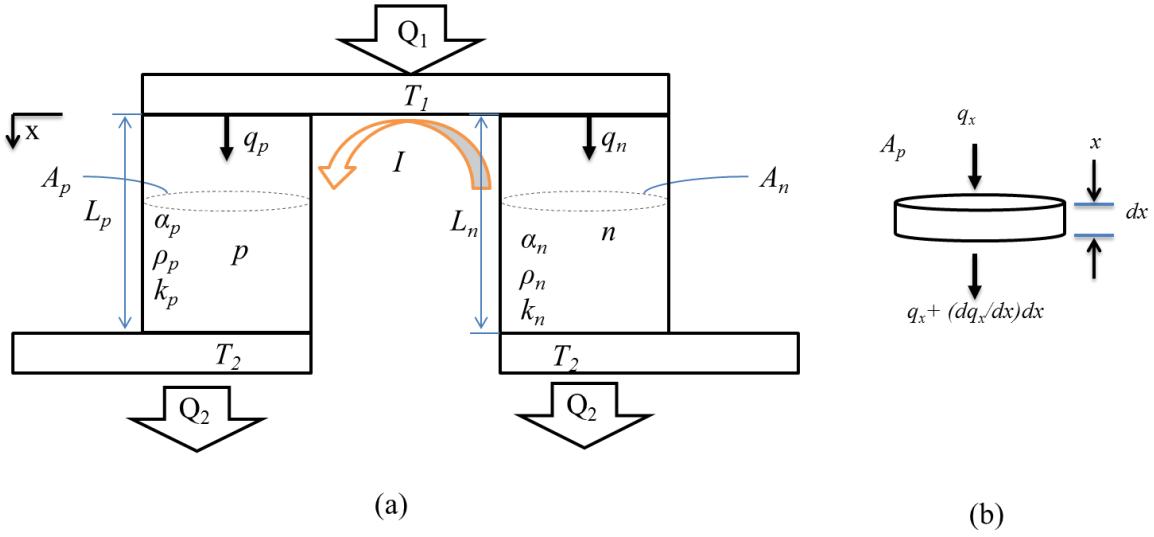

Figure 2.1. (a) Schematic of thermoelectric couple, (b) differential element. [2]

$$\dot{Q}_1 = q_p + q_n \qquad 2.1$$

The heat flows for p-type and n-type materials are equal to the Peltier heat and Fourier's law of conduction (thermal conduction) that can be written as follows

$$q_p = \alpha_p T_1 I + \left(-k_p A_p \frac{dT}{dx}\Big|_{x=0}\right) \qquad 2.2$$

$$q_n = -\alpha_n T_1 I + \left(-k_n A_n \frac{dT}{dx}\Big|_{x=0}\right) \qquad 2.3$$

In order to obtain the temperature gradient along *x*, the heat balance is applied on a differential element as shown in Figure 2.1 (b) as follows

$$\underbrace{q_x - \left(q_x + \frac{dq_x}{dx}dx\right)}_{\substack{heat\ transfer \\ across\ the\ surface \\ of\ the\ element}} + \underbrace{\frac{I^2\rho_p}{A_p}dx}_{Joul\ heating} = 0 \qquad 2.4$$

$$-\frac{d}{dx}\left(-k_p A_p \frac{dT}{dx}\right) + \frac{I^2\rho_p}{A_p} = 0 \qquad 2.5$$

After integrating the above equation twice from 0 to L_p, the temperature gradient at $x = 0$ is

$$\left.\frac{dT}{dx}\right|_{x=0} = -\frac{I^2\rho_p L_p}{2A_p^2 k_p} - \frac{(T - T_2)}{L_p} \qquad 2.6$$

Substituting the above equation into equation 2.2 gives

$$q_p = \alpha_p T\ I - \frac{1}{2}I^2\frac{\rho_p L_p}{A_p} + \frac{k_p A_p}{L_p}(T - T_2) \qquad 2.7$$

The heat transfer for the n-type material can be obtained in a similar way

$$q_n = -\alpha_n T\ I - \frac{1}{2}I^2\frac{\rho_n L_n}{A_n} + \frac{k_n A_n}{L_n}(T - T_2) \qquad 2.8$$

As a result, equation 2.1 becomes

$$\dot{Q} = (\alpha_p - \alpha_n)T\ I - \frac{1}{2}I^2\left(\frac{\rho_p L_p}{A_p} + \frac{\rho_n L_n}{A_n}\right) + \left(\frac{k_p A_p}{L_p} + \frac{k_n A_n}{L_n}\right)(T - T_2) \quad 2.9$$

Moreover,

$$\alpha = \alpha_p - \alpha_n \quad 2.10$$

$$R = \frac{\rho_p L_p}{A_p} + \frac{\rho_n L_n}{A_n} \quad 2.11$$

$$K = \frac{k_p A_p}{L_p} + \frac{k_n A_n}{L_n} \quad 2.12$$

As a result, equation 2.9 becomes

$$\dot{Q} = \alpha T\ I - \frac{1}{2}I^2 R + K(T - T_2) \quad 2.13$$

Similarly, by using the energy balance equations at junction temperature T_2, $\dot{Q}_2$ becomes

$$\dot{Q}_2 = \alpha T_2 I + \frac{1}{2}I^2 R + K(T - T_2) \quad 2.14$$

In an ideal case, the current in equations 2.13 and 2.14 can either be supplied to the couple or generated depending on the direction of the heat flow. For the same direction shown in *Figure 2.1* (a), the thermocouples represent the thermoelectric generator if the current is being obtained and thermoelectric cooler if the current is being supplied. [2]

2.1.2 Thermoelectric Generator [2]

A thermoelectric generator is a power-generating device that directly converts thermal energy to electrical energy. When the connected junctions of two dissimilar materials (n-type and p-type) have a temperature difference, an electrical current is generated as shown in Figure 2.2. For a thermoelectric generator, state 1 in equation 2.13 and 2.14 is used for the hot side and state 2 is for the cold side as shown below

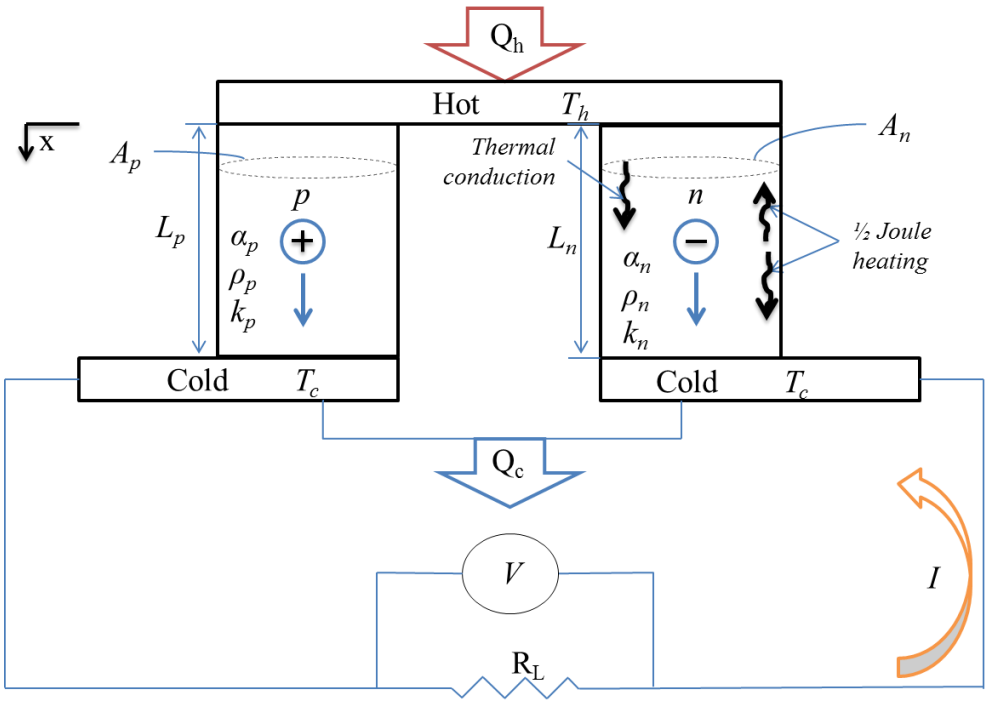

Figure 2.2 .An electrical circuit for a unit couple of a thermoelectric generator

$$\dot{Q}_h = \alpha T_h I - \frac{1}{2} I^2 R + K(T_h - T_c) \qquad 2.15$$

$$\dot{Q}_c = \alpha T_c I + \frac{1}{2} I^2 R + K(T_h - T_c) \qquad 2.16$$

By applying the first law of thermodynamics, the electric power $\dot{W}$ generated from the thermocouple is

$$\dot{W} = \dot{Q}_h - \dot{Q}_c \tag{2.17}$$

or

$$\dot{W} = \alpha I(T_h - T_c) - I^2 R \tag{2.18}$$

Also,

$$\dot{W} = I^2 R_L \tag{2.19}$$

where R_L is the load resistance. Moreover, Ohm's Law is defined as

$$V = IR_L = \alpha(T_h - T_c) - IR \tag{2.20}$$

Therefore, current I is equal to

$$I = \frac{\alpha(T_h - T_c)}{R_L + R} \tag{2.21}$$

The thermal efficiency of the thermoelectric generator is defined as the ratio of power output to the heat input

$$\eta_{th} = \frac{\dot{W}}{\dot{Q}_h} \tag{2.22}$$

$$\eta_{th} = \frac{I^2 R_L}{\alpha T_h I - \frac{1}{2} I^2 R + K(T_h - T_c)} \tag{2.23}$$

The output power and thermal efficiency can also be rewritten in terms of R_L/R as follows

$$\dot{W} = \frac{\alpha^2 T_c^2 \left[\left(\frac{T_c}{T_h}\right)^{-1} - 1\right]^2 \left(\frac{R_L}{R}\right)}{R\left(1 + \frac{R_L}{R}\right)^2} \tag{2.24}$$

$$\eta_{th} = \frac{\left(1 - \frac{T_c}{T_h}\right)\left(\frac{R_L}{R}\right)}{\left(1 + \frac{R_L}{R}\right) - \frac{1}{2}\left(1 - \frac{T_c}{T_h}\right) + \frac{\left(1 + \frac{R_L}{R}\right)^2 \frac{T_c}{T_h}}{ZT_c}} \quad 2.25$$

For maximum conversion efficiency

$$\frac{d\eta_{th}}{d\left(\frac{R_L}{R}\right)} = 0 \quad \xrightarrow{gives} \quad \frac{R_L}{R} = \sqrt{1 + Z\bar{T}} \quad 2.26$$

where $\bar{T}$ is the average temperature between the hot and cold junction and is equal to

$$\bar{T} = \frac{T_c + T_h}{2} = \frac{1}{2} T_c \left[1 + \left(\frac{T_c}{T_h}\right)^{-1}\right] \quad 2.27$$

As a result, the maximum conversion efficiency, η_{mc}, is

$$\eta_{mc} = \left(1 - \frac{T_c}{T_h}\right) \frac{\sqrt{1 + Z\bar{T}} - 1}{\sqrt{1 + Z\bar{T}} + \frac{T_c}{T_h}} \quad 2.28$$

For maximum power efficiency

$$\frac{d\dot{W}}{d\left(\frac{R_L}{R}\right)} = 0 \quad \xrightarrow{gives} \quad \frac{R_L}{R} = 1 \quad 2.29$$

As a result, the optimum current, I_{mp}, for maximum power, $\dot{W}_{max}$ and maximum power efficiency, η_{mp}, are

$$I_{mp} = \frac{\alpha \Delta T}{2R} \quad 2.30$$

$$\dot{W}_{max} = \frac{\alpha^2 \Delta T^2}{4R} \quad 2.31$$

$$\eta_{mp} = \frac{\left(1 - \frac{T_c}{T_h}\right)}{2 - \frac{1}{2}\left(1 - \frac{T_c}{T_h}\right) + \frac{4\frac{T_c}{T_h}}{ZT_c}} \qquad 2.32$$

It can be seen from the above equations that the maximum parameters I_{mp}, $\dot{W}_{max}$, and η_{mp} are independent of the load resistance, R_L. Therefore, these maximum parameters can be used to generate a generalized graph for TEG as a function of load resistance where output power, voltage, electrical current, and thermal efficiency obtained from equations 2.19, 2.20, 2.21, and 2.23, respectively, are divided by maximum parameters as shown Figure 2.3. It can be seen from the plot that the maximum output power is when the load resistance is equal to the internal resistance of the thermoelectric couple. Moreover, the thermal efficiency curve follows the same trend of the output power, but its maximum value does not appear when the load resistance is equal to the internal resistance.

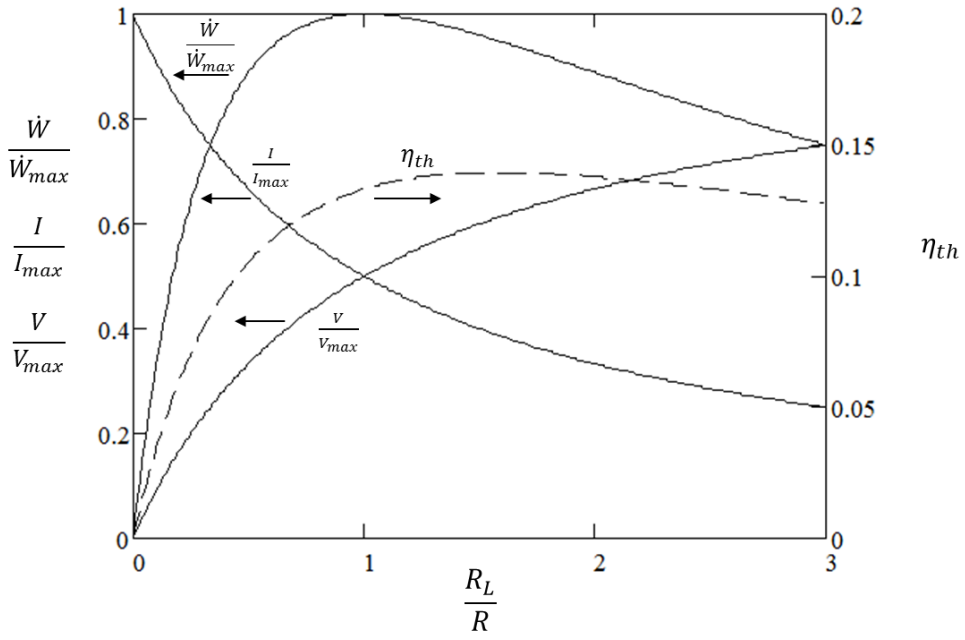

Figure 2.3. Generalized chart of TEG characteristics with the assumptions of $\boldsymbol{Z\overline{T} = 1}$ and $\boldsymbol{T_c/T_h = 0.5}$

The previous analyses represent the concepts of the thermoelectric generator of one thermocouple where multiple couples are being used in many of the TEG applications. In order to obtain the thermoelectric parameters for multiple couples (TE modules as shown in Figure 2.4), the unit couple parameters need to be multiplied by the number of couples, n, as follows

$$\left(\dot{W}\right)_{no} = n\dot{W} \quad 2.33$$

$$\left(\dot{Q}_h\right)_{no} = n\dot{Q}_h \quad 2.34$$

$$(R)_{no} = nR \quad 2.35$$

$$(R_L)_{no} = nR_L \quad 2.36$$

$$(V)_{no} = nV \quad 2.37$$

$$(K)_{no} = nK \quad 2.38$$

$$(I)_{no} = I \quad 2.39$$

$$(\eta_{th})_{no} = \frac{\left(\dot{W}\right)_{no}}{\left(\dot{Q}_h\right)_{no}} = \eta_{th} \quad 2.40$$

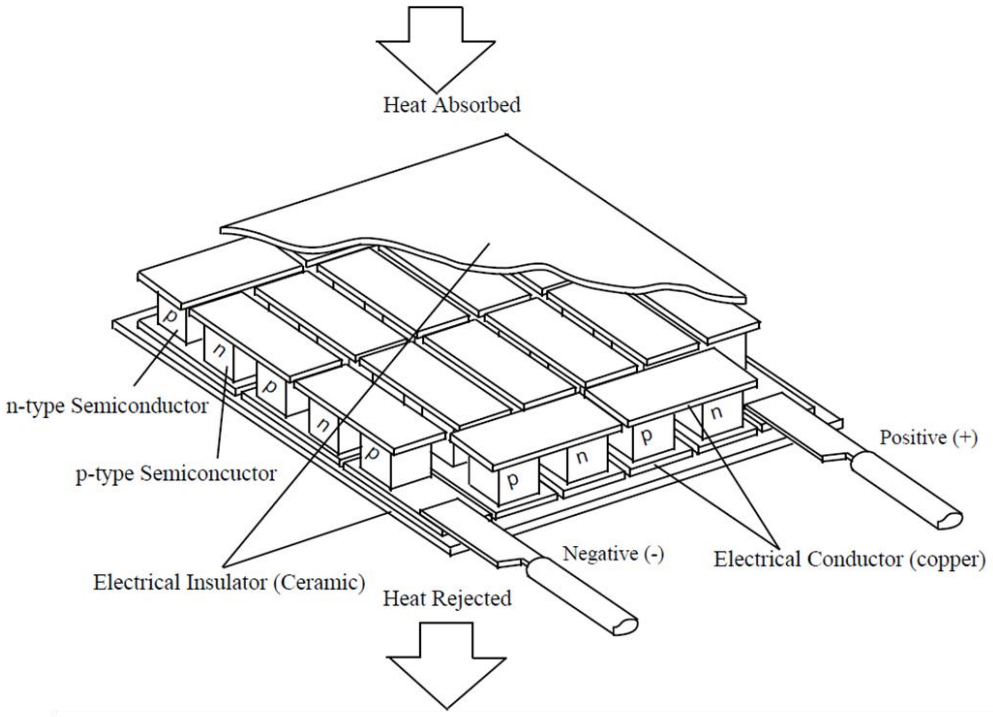

Figure 2.4. Cutaway of a typical thermoelectric module where the orientation of multicouples is shown. [13]

2.1.3 Thermoelectric Cooler (TEC)

The Seebeck effect is a reversible process; i.e., if a current is supplied to a thermoelectric couple, electrons and holes will move through *p* and *n* elements causing heating on one side and cooling on the other as shown in Figure 2.5.

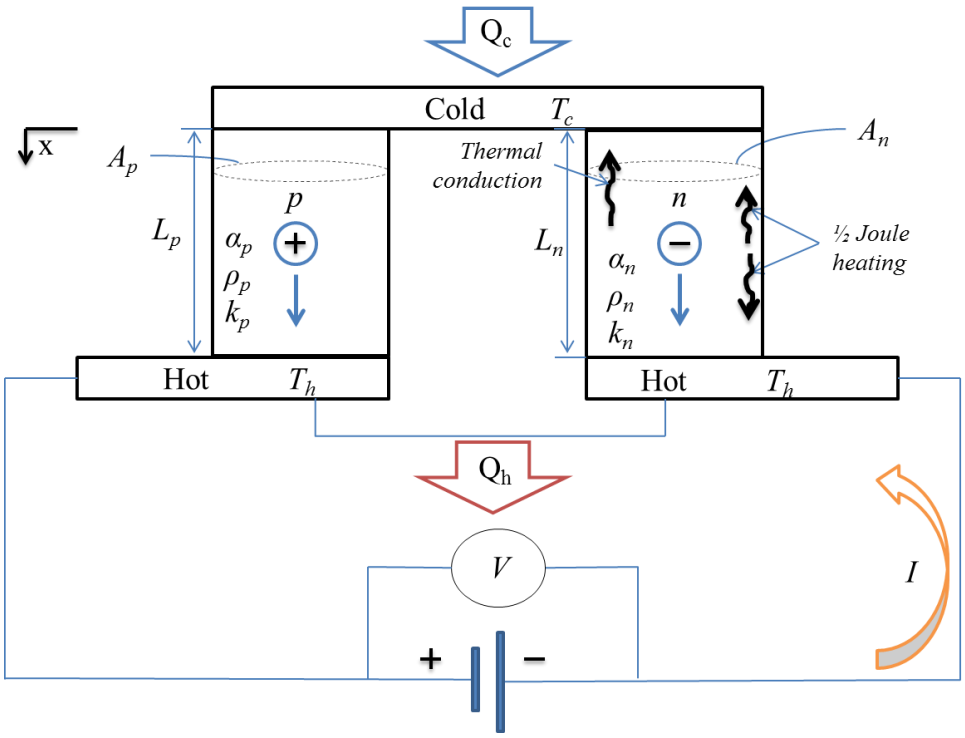

Figure 2.5. An electrical circuit for a unit couple thermoelectric cooling.

For thermoelectric cooling, state 1 and 2 used in equations 2.13 and 2.14 denote cold and hot side respectively which gives [2]

$$\dot{Q}_c = \alpha T_c I - \frac{1}{2} I^2 R + K(T_c - T_h) \qquad 2.41$$

$$\dot{Q}_h = \alpha T_h I + \frac{1}{2} I^2 R + K(T_c - T_h) \qquad 2.42$$

By applying the first law of thermodynamics across the thermocouple, the input power can be defined as

$$\dot{W} = \dot{Q}_h - \dot{Q}_c \tag{2.43}$$

which is also equal to

$$\dot{W} = \alpha I(T_h - T_c) + I^2R \tag{2.44}$$

also,

$$\dot{W} = IV \tag{2.45}$$

and voltage becomes

$$V = \alpha(T_h - T_c) + IR \tag{2.46}$$

The coefficient of performance, COP, is similar to the thermal efficiency but its value may exceed unity and it is defined as the ratio of the cooling power (or heating power) to the input power. [2]

$$COP = \frac{\dot{Q}_c}{\dot{W}} \tag{2.47}$$

Substituting equations 2.41 and 2.44 into 2.47 gives [12]

$$COP = \frac{\alpha T_c I - \frac{1}{2} I^2 R - K\Delta T}{\alpha I \Delta T + I^2 R} \tag{2.48}$$

where

$$\Delta T = (T_h - T_c) \tag{2.49}$$

For maximum cooling power, $\dot{Q}_{c,mp}$, the optimum input current can be found by differentiating equation 2.41 with respect to current and setting it to zero as follows [12]

$$\frac{d\dot{Q}_c}{dI} = \alpha T_c - IR = 0 \xrightarrow{gives} I_{mp} = \frac{\alpha T_c}{R} \tag{2.50}$$

The current in equation 2.50 can also be represented in terms of T_h [12]

$$I_{max} = \frac{\alpha(T_h - \Delta T_{max})}{R} \qquad 2.51$$

The maximum temperature difference ΔT_{max} is the maximum possible difference in temperature which always occurs when the cooling power is at zero and the current is maximum. This is obtained by setting $\dot{Q}_c = 0$ in equation 2.41, substituting both I and T_c by I_{max} and $T_h - \Delta T_{max}$, respectively, and solving for ΔT_{max}. The maximum temperature difference is obtained as [12]

$$\Delta T_{max} = \left(T_h + \frac{1}{Z}\right) - \sqrt{\left(T_h + \frac{1}{Z}\right)^2 - T_h^2} \qquad 2.52$$

where the figure of merit Z (unit: K^{-1}) is defined as [12]

$$Z = \frac{\alpha^2}{\rho k} = \frac{\alpha^2}{RK} \qquad 2.53$$

The maximum cooling power $\dot{Q}_{c,max}$ is the maximum thermal load which occurs at $\Delta T = 0$ and $I = I_{max}$. This can be obtained by substituting both I and T_c in equation 2.41 by I_{max} and $T_h - \Delta T_{max}$, respectively, and solving for $\dot{Q}_{c,max}$. The maximum cooling power for a thermoelectric module with n thermoelectric couples is [12]

$$\dot{Q}_{c,max} = \frac{n\alpha^2(T_h - \Delta T_{max})}{2R} \qquad 2.54$$

The maximum voltage is the DC voltage, which delivers the maximum possible temperature difference ΔT_{max} when $I = I_{max}$. The maximum voltage is obtained from equation 2.46, which is [12]

$$V_{max} = n\alpha T_h \qquad 2.55$$

The maximum COP can be obtained by differentiating equation 2.48 with respect to current and setting it to zero as follows [12]

$$\frac{d(COP)}{dI} = 0 \xrightarrow{gives} I_{COP} = \frac{\alpha \Delta T}{R\left[(1+Z\bar{T})^{\frac{1}{2}} - 1\right]} \qquad 2.56$$

$$COP_{max} = \frac{T_c}{T_h - T_c} \frac{(1+Z\bar{T})^{\frac{1}{2}} + \frac{T_h}{T_c}}{(1+Z\bar{T})^{\frac{1}{2}} + 1} \qquad 2.57$$

where

$$Z\bar{T} = ZT_h\left(1 - \frac{\Delta T}{2T_h}\right) \qquad 2.58$$

A dimensionless cooling power ($\dot{Q}_c/\dot{Q}_{c,max}$) and COP vs. dimensionless current (I/I_{max}) can be presented graphically as shown in Figure 2.6 assuming $ZT_c = 1$. The dimensionless cooling power is obtained from the cooling power found in equation 2.41 , where the current is the only variable, and from the maximum cooling power equation (2.54) at given thermoelectric material properties and hot side temperature. This generalized plot shows that the cooling power is inversely proportional to the coefficient of performance especially at smaller temperature difference. Moreover, increasing the temperature difference across the junction will decrease the cooling power and the performance of the TEC. [12]

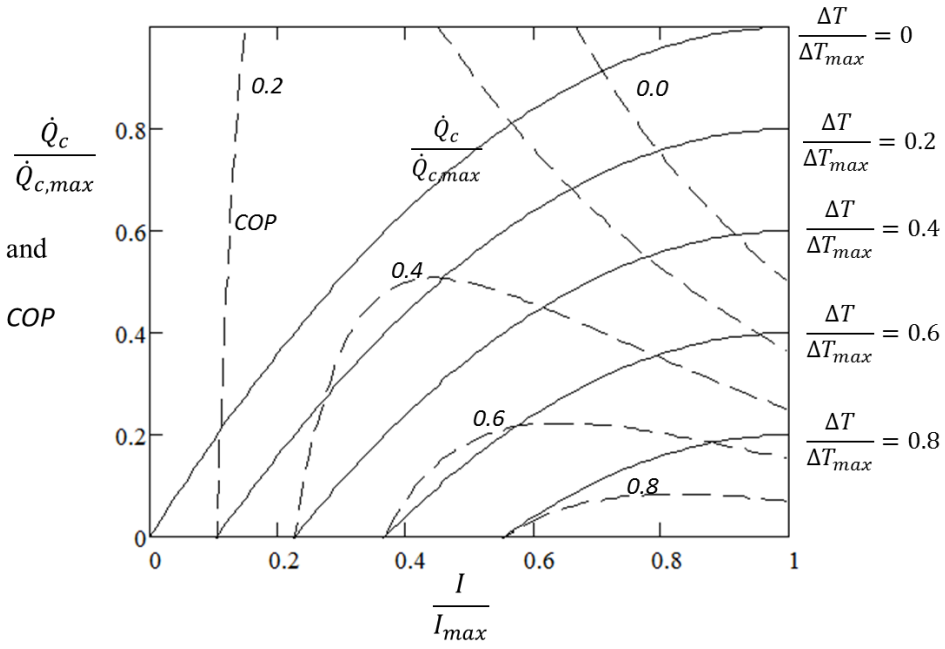

Figure 2.6. Generalized chars for TEC assuming $\boldsymbol{ZT_c = 1}$

Similar to the thermoelectric generator, the thermoelectric cooler parameters for multiple couples can be obtained by from the unit couple parameters and the number of couples, n, as follow [2]

$$\left(\dot{Q}_c\right)_n = n\dot{Q}_c \qquad 2.59$$

$$\left(\dot{Q}_h\right)_n = n\dot{Q}_h \qquad 2.60$$

$$\left(\dot{W}\right)_n = n\dot{W} \qquad 2.61$$

$$(R)_n = nR \qquad 2.62$$

$$(V)_n = nV \qquad 2.63$$

$$(K)_n = nK \qquad 2.64$$

$$(I)_n = I \qquad 2.65$$

$$(COP)_n = \frac{(\dot{Q}_c)_n}{(\dot{W})_n} = COP \qquad 2.66$$

2.2 Contact Resistances

The thermocouples are usually connected in series by highly conductive metal strips. A number of thermocouples are connected electrically in series and sandwiched between (thermally conducting but electrically insulating) ceramic plates as shown in Figure 2.7. These conductors add electrical and thermal resistances to the system, which sometimes increase the discrepancies between the realistic and ideal equation models.

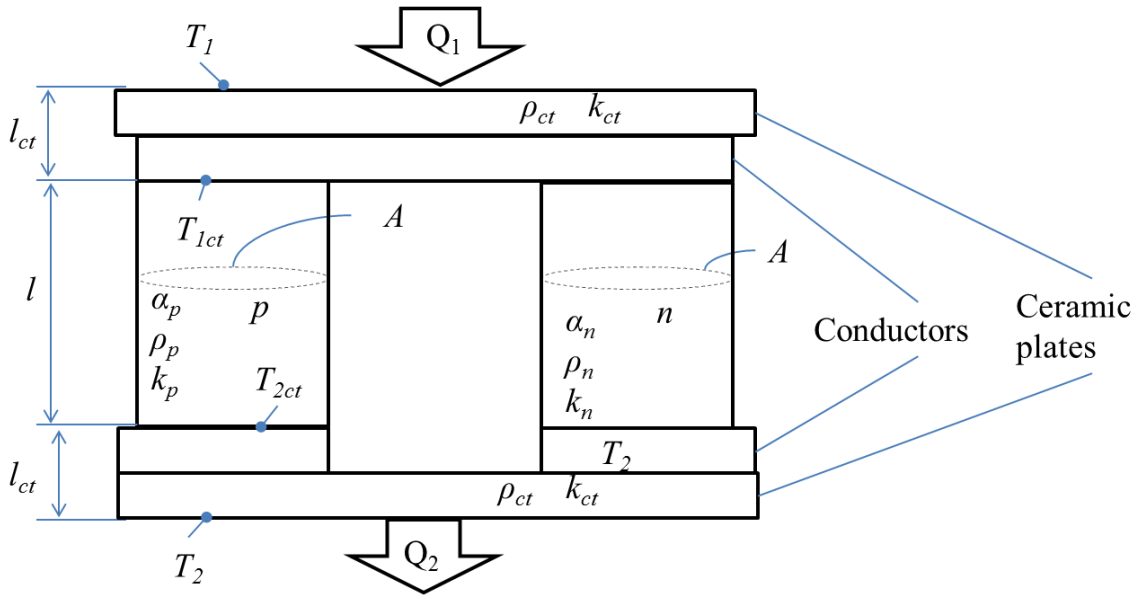

Figure 2.7. Basic configuration of a real thermoelectric couple. [2]

Consider a single couple thermoelectric cooler where the steady state heat balance can be written as [2]

$$\dot{Q}_1 = \frac{Ak_{ct}}{l_{ct}}(T_1 - T_{1ct}) \qquad 2.67$$

$$\dot{Q}_1 = \alpha I T_{1ct} - \frac{1}{2} I^2 R - \frac{Ak}{l}(T_{2ct} - T_{1ct}) \quad 2.68$$

$$\dot{Q}_2 = \alpha I T_{2ct} + \frac{1}{2} I^2 R - \frac{Ak}{l}(T_{2ct} - T_{1ct}) \quad 2.69$$

$$\dot{Q}_2 = \frac{Ak_{ct}}{l_{ct}}(T_{2ct} - T_2) \quad 2.70$$

where k_{ct} is the thermal contact conductivity which includes the thermal conductivity of the ceramic plates and thermal contacts and l_{ct} is the thickness of the contact layer. The electrical resistance is composed of the thermocouple and electrical contact resistances as follows [2]

$$R = R_o + R_{ct} = \frac{\rho l}{A} + \frac{\rho_{ct}}{A} = \frac{\rho l}{A}\left(1 + \frac{s}{l}\right) \quad 2.71$$

where ρ is the electrical resistivity and it is equal to $\rho_n + \rho_p$, ρ_{ct} is the electrical contact resistivity, and s is the ratio between the electrical contact resistivity and electrical resistivity ($s = \rho_{ct}/\rho$). Equations 2.67 to 2.70 are rearranged to have the cooling power per unit area and the coefficient of performance of the TEC module to be [2]

$$\frac{\dot{Q}_1}{nA} = \frac{kT_1}{l}\left[\frac{2Z\bar{T}\xi_{TEC}\left(\frac{T_1}{T_2}+1\right)^{-1}\left(\frac{T_1}{T_2}-1\right)}{\psi\left(1+\frac{s}{l}\right)\left(1-mr\frac{l_c}{l}\right)} - \frac{Z\bar{T}\left(\frac{T_2}{T_1}+1\right)^{-1}\left(\frac{T_1}{T_2}-1\right)^2}{\psi^2\left(1+\frac{s}{l}\right)\left(1-mr\frac{l_c}{l}\right)^2} - \frac{\left(\frac{T_1}{T_2}-1\right)}{\left(1-mr\frac{l_c}{l}\right)}\right] \quad 2.72$$

$$COP = \frac{\xi_{TEC}\left(1 - mr\frac{l_c}{l}\right)}{\frac{T_2}{T_1} - 1}\frac{\left[\psi - \frac{\frac{T_2}{T_1} - 1}{2\xi_{TEC}\left(1 - mr\frac{l_c}{l}\right)} - \frac{\psi^2\left(\frac{T_2}{T_1} + 1\right)\left(1 + \frac{s}{l}\right)}{2Z\bar{T}\xi_{TEC}}\right]}{\psi + 1} \quad 2.73$$

where

$$r = k/k_c \quad 2.74$$

$$m = 2\left(\frac{Z\bar{T}}{\psi\left(1 + \frac{s}{l}\right)} - 1\right) \quad 2.75$$

$$\psi = \sqrt{1 + Z\bar{T}} - 1 \quad 2.76$$

$$\xi_{TEC} = \frac{T_{1c}}{T_1} = \frac{1 + \frac{l_c}{l}\frac{Z\bar{T}\left(1 + \frac{T_2}{T_1}\right)^{-1}\left(\frac{T_2}{T_1} - 1\right)^2}{\psi^2\left(1 + \frac{s}{l}\right)\left(1 - mr\frac{l_c}{l}\right)^2} + r\frac{l_c}{l}\frac{\left(\frac{T_2}{T_1} - 1\right)}{\left(1 - mr\frac{l_c}{l}\right)}}{1 + 2r\frac{l_c}{l}\frac{Z\bar{T}\left(1 + \frac{T_2}{T_1}\right)^{-1}\left(\frac{T_2}{T_1} - 1\right)}{\psi\left(1 + \frac{s}{l}\right)\left(1 - mr\frac{l_c}{l}\right)}} \quad 2.77$$

After studying the above equations, it is found that the effect of the contact resistances increases as the length of the element is decreased. Figure 2.8 shows the cooling power per unit area ($\dot{Q}_1/nA$) presented in equation 2.72 and COP (equation 2.73) as a function of the length of the element for four different values of *r*. The figure implies that the greater the contact resistances the smaller the TEC performances. Moreover, the decreasing length of the element implies a greater

discrepancy from using the ideal equations (when r and s are equal to zero) especially when the length of the element is less than $0.1mm$. [2]

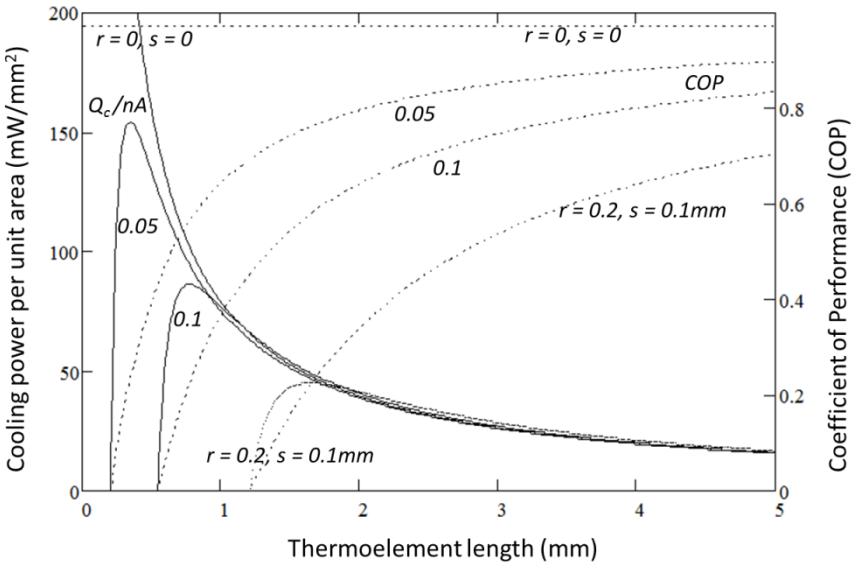

Figure 2.8. Cooling power per unit area and COP as a function of thermoelement length for different values of $\boldsymbol{r}$ and when $\boldsymbol{s = 0.1mm}$, $\boldsymbol{\psi = 0.2}$, $\boldsymbol{k = 1.5W/mK}$, $\boldsymbol{l_c = 0.1mm}$, $\boldsymbol{T_1 = 275K}$, $\boldsymbol{T_2 = 300K}$, and $\boldsymbol{Z = 3 \times 10^{-3}\ K^{-1}}$. [2]

2.3 Thermoelectric System

The typical thermoelectric system is usually attached to heat sinks or heat exchanger devices in order to improve the heat absorption and/or rejection. Once these heat sinks are attached, new equations will be considered along with the ideal equations discussed earlier.

2.3.1 Basic Equations

Under steady-state heat transfer, consider the thermoelectric cooler system shown in Figure 2.9. Each heat sink faces a fluid flow at temperature T_∞. Subscript 1 and 2 denote the entities of fluid 1 and 2, respectively. Consider that an electric current is

directed in a way that the cooling power $\dot{Q}_1$ enters heat sink 1. We assume that the electrical and thermal contact resistances in the TEC are negligible, the material properties are independent of temperature, the TEC is perfectly insulated, and the p-type and n-type element dimensions are identical. [10]

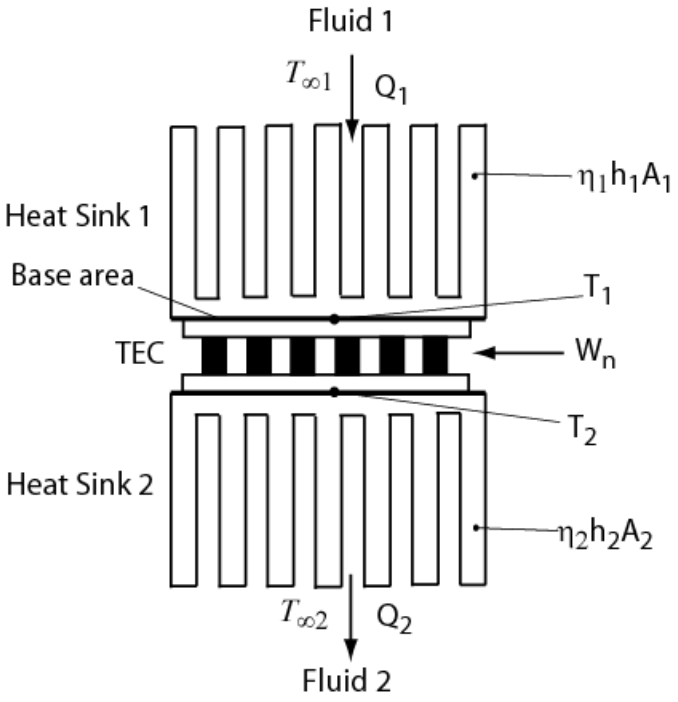

Figure 2.9. Thermoelectric cooler module attached to two heat sinks.

The basic equations for the TEC with two heat sinks are given by

$$\dot{Q}_1 = \eta_1 h_1 A_1 (T_{\infty 1} - T_1) \tag{2.78}$$

$$\dot{Q}_1 = n\left[\alpha I T_1 - \frac{1}{2} I^2 R + \frac{A_e k}{L_e}(T_1 - T_2)\right] \tag{2.79}$$

$$\dot{Q}_2 = n\left[\alpha I T_2 + \frac{1}{2} I^2 R + \frac{A_e k}{L_e}(T_1 - T_2)\right] \tag{2.80}$$

$$\dot{Q}_2 = \eta_2 h_2 A_2 (T_2 - T_{\infty 2}) \qquad 2.81$$

It is noted that the thermal resistances of the heat sinks can be expressed by the reciprocal of the convection conductance (i.e., $\eta_1 h_1 A_1$, where η_1 is the fin efficiency, h_1 is the convection coefficient, and A_1 is the total surface area of the cold heat sink). Also, A_e is the element cross-sectional area, L_e is the element length, and T_1 and T_2 are the heat sinks' 1 and 2 base temperatures respectively which are equal to the thermoelectric module junctions temperatures. [10]

2.4 Heat Sink Design and Optimization

The purpose of attaching a heat sink to the thermoelectric module is to maximize the heat transfer rate from the fins. Therefore, at the given dimensions (width, W_f, length, L_f, and profile length, b_f) shown in Figure 2.10, the objective of this section is to optimize the fin thickness, t_f, and fin spacing, z_f of a heat sink in order to minimize the thermal resistance.

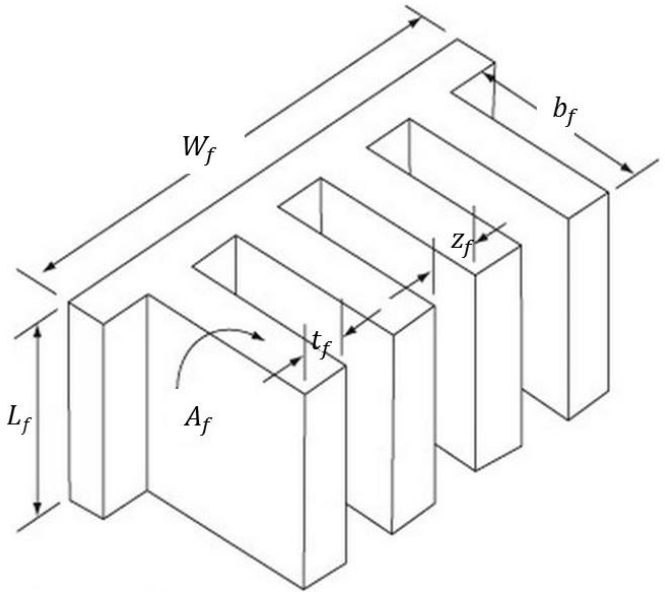

Figure 2.10. Multiple array heat sink. [2]

The total fin efficiency is a well-known parameter used to analyze the heat sink thermal resistance and it is defined as follows [2]

$$\eta_f = \frac{\tanh\left[b_f\left(\frac{2h}{k_f t_f}\right)^{1/2}\right]}{b_f\left(\frac{2h}{k_f t_f}\right)^{1/2}} \qquad 2.82$$

where k_f is the thermal conductivity of the fin and h is the heat transfer coefficient of the fluid which can be found from the Nusselt number correlation, Nu, as follow

$$h = \frac{k_{fluid}}{L_f} Nu \qquad 2.83$$

where k_{fluid} is the thermal conductivity of the fluid and L_f is the length of the heat sink that can be replaced by the hydraulic diameter, D_h, for channel flow case. The total heat transfer area of the heat sink is given by

$$A_f = n_f\left[2\left(L_f + t_f\right) + L_f z_{f,opt}\right] \quad 2.84$$

where n_f is the number of fins. Moreover, it is found that the optimum fin spacing is equal to

$$z_{f,opt} = 3.24 L_f Re_L^{-1/2} Pr^{-1/4} \quad 2.85$$

where Re_L is the Reynolds number for flow over a plate and Pr is the Prandtl number. After finding the optimum fin spacing for given heat sink parameters, the fin thickness can be optimized to give the maximum heat transfer as follows

$$q_f = \eta_f h A_f (T_\infty - T_b) \quad 2.86$$

where T_∞ and T_b are the fluid temperatures and the heat sink base temperature respectively. [2]

2.5 Chapter Conclusion

Chapter 2 discusses most of the concepts that are needed to understand the fundamentals of thermoelectrics from a thermal design perspective. These concepts are essential to understand and study the current work. After that, the literature of TEAC system can be studied in order to figure out the current status and investigate if there's any room for further improvement.

CHAPTER 3

LITERATURE REVIEW AND THE OBJECTIVE OF THE STUDY

The goals of this chapter are to discuss the state of art of the current study and sort its objective. The literature review section focuses on TEAC system and related subjects that are needed for the current study. After studying the basic concepts of thermoelectrics, it is found that a typical air-type thermoelectric system should be attached to a heat sink in order to have a lower thermal resistance. Therefore, finding a reliable method that shows how the optimum heat sink parameters and appropriate Nusselt number correlation are obtained plays a great role in discovering an accurate optimum design of TEAC. Moreover, the availability of the optimum design of the thermoelectric system also should be investigated, since the thermoelectric system has several parameters where some of them need to be optimized simultaneously. Finally, the optimum design of the current work is investigated analytically and experimental validation might be required where it is needed to find out how the experiment is being conducted in the literature. After summarizing the literature review, the objective of this work now can be addressed as shown in section 3.2.

3.1 Literature Review

3.1.1 TEAC System

The literature showed a number of studies on TEAC. The first mention of automotive TEAC system was presented by Uemura [14] in Japan back in 1958 where a thermoelectric air conditioner system was built in the trunk of a car made by Chrysler. A fFew decades later, Junior et al. [15] studied and compared a gas-to-liquid TEAC system used for steady state and transient models with the conventional auto HVAC system. They used a model from the object-oriented Modelica library TIL and validated this model against experimental data of a prototype heat exchanger. For room temperature, the HVAC system has the capacity to pump heat five times higher than the TEAC system at the same input power.

Wang et al. [16] designed, analyzed, and tested an air-to-liquid TEAC system for a passenger vehicle using a numerical model. The numerical model was used to optimize a combination of up to 14 variables in order to achieve the best TEAC performance. The experimental results validated the simulated one and showed a *COP* of 1.55 at a cooling power of 1.55 kW with air and liquid inlet temperatures of 30°C. They applied the thermal isolation method [11] which allowed them to improve the *COP* and obtain the fluid and junction temperatures [16].

Raut and Walke [17] built and tested a TEAC system inside a small passenger vehicle where the goal was to pump 222 W of heat from the cabin. Their system, which consists of six TEC modules connected electrically in series sandwiched between two heat sinks, can reduce the cabin temperature to as low as 7°C. The system is designed to recirculate the cold air to improve the efficiency and have a cabin temperature of 25^{o}C

where the ambient temperature is about 32^{o}C. The COP of their system is about 0.77 and it is calculated by dividing the cooling capacity by the input power (the product of the input current and voltage).

Hsu et al. [18] studied and tested an air-to-liquid TEAC installed in a vehicle (Honda Civic Exi) where they used an optimized heat sink. They also studied the effects of the figure of merit and the element thickness on the cooling performances where they indicated that the change of the pallet thickness can improve the cooling power but not the *COP*. Their experimental results validated the analytical model using the basic equations.

In the 2012 Directions in Engine-Efficiency and Emissions Research (DEER) Conference, Gentherm collaborated with the Ford Motor Company and presented their design of a TEAC along with a performance curve [9]. At an input power of 400 W, their air-to-liquid TEAC system was able to reach a COP of 1.3 using a cold air flow rate of 60 CFM and ambient cold and hot temperatures of 30^{o}C. Many advantages encouraged them to decide on using liquid instead of air for the hot (waste) side fluid specially the advantage of having a higher heat transfer coefficient [19]. Table 3.1 highlights more pros and cons of air-to-air vs. air-to-liquids TEAC systems.

Table 3.1

Comparison Between Air-to-air TEAC and Air-to-liquid TEAC. [19]

Air Waste Stream		Liquid Waste Stream	
Pros	**Cons**	**Pros**	**Cons**
Low weight	Poor heat transfer	Higher power density	More weight
No risk of coolant leaks	Lower power density	Less noise	Risk of leaks
	Difficult to vent the waste heat		Requires an additional radiator
	Noise at higher flow rate		Waste side temp tied to ambient

3.1.2 Heat Sink Optimization and Its Heat Transfer Coefficient

A typical thermoelectric system consists of a thermoelectric module and two heat exchangers (or heat sinks) attached to both the hot and cold side of the module. It can be seen that the researchers make an effort to combine theoretical thermoelectric equations and heat sinks equations, and then optimize the geometric parameters of the heat sinks [20]. Optimization of the heat sinks and heat exchangers are very well established in the literature and Lee [2] summarizes a comprehensive study on the optimization procedures. As for the accuracy of the Nusselt number, analytical correlation can be used, but it would be more reliable to have an experimental validation, especially for more complicated shapes [21]. Therefore, Teertstra et al. [22] developed an analytical correlation to calculate the Nusselt number based on flow in a parallel plate channel and a combination of developing and fully developed flow. After modifying the Nusselt number correlation to consider the fin effects, they compared the new correlation with

experimental values which showed good agreement. Furthermore, Zhimin and Fah [23] used two correlations to calculate the Nusselt number for microchannel heat sinks for both laminar and turbulent flow. The results of the thermal resistances were then validated against other work. These studies of the heat sink optimization and Nusselt number correlation can be adopted on the current work on thermoelectric system.

3.1.3 Optimum Design of Thermoelectric System

The state-of-art related projects of thermoelectric parameters, on the other hand, need to be addressed in order to investigate their optimum design. Literature shows serval general methods (or in a different areas) on how to optimize thermoelectric parameters. Analyzing the product of the number of thermocouples, the element geometric ratio, and the thermal conductivity, which is defined as the thermal conductance of elements, is a very practical way to assist studying the optimum design of the thermoelectric parameters [10]. The literature also showed some techniques that can help analyze the optimum design of the thermoelectric parameters.

Dimensionless parameters for a thermoelectric cooler system were introduced by Yamanashi [24] in order to optimize thermoelectric parameters. The paper studied the effect of different dimensionless parameters on the TEC performance as a function of dimensionless electrical current. One of the highlights of this paper is to show that the thermal resistance of the hot side of the TEC has a greater impact on the performance than the cold side thermal resistance. Furthermore, this technique gives the ability to obtain the maximum COP when the heat exchanger of the TEC system is provided. Even though the Yamanashi technique is not very adoptable due to the difficulties in obtaining the optimum parameters for the cooling power, some researchers applied it and provide

useful results. In fact, Xuan [25] was able to use the Yamanashi method to optimize the length of the element while Pan et al. [26] studied the optimum design of cooling power for a thermoelectric cooler.

There are also more studies on the investigation of the optimum design of thermoelectric system but applying these methods does not seem very practical. One example is the comparison of the power density of the waste exhaust heat recovery when using a thermoelectric generator system. For similar inputs, the reported power densities of Hsu et al. [27], and later, Karri et al. [28], and New Energy and Industrial Technology Development Organization (NEDO) [29] are 0.032 W/cm^2, 0.61 W/cm^2, and $1W/cm^2$, respectively. These variations in the power densities raised the question of the availability of the optimum design of the thermoelectric system.

Lately, Lee [10] developed an optimal design method that uses the dimensional analysis to optimize the thermoelectric generator and cooler parameters. For thermoelectric cooler, the method gives the ability to optimize the electrical current and the geometric ratio (thermoelement cross sectional area by its length) simultaneously at a given figure of merit, ambient temperatures, and heat sink parameters. This method will be adopted in the current study in order to develop the optimum design of the TEAC which will be discussed in the next chapter.

3.1.4 Experimental Work of Thermoelectric system

Apart from the optimum design literature, the above summary focuses on the theoretical approach of a thermoelectric system. After that, the concern appeared on how accurate these equations were when they are compared with experiment. The literature showed some experimental works that studied the validation of the theoretical equations.

The formulated equations found by Chen et al. [30] were experimentally validated by Gou et al. [31] when they tested a low temperature waste heat recovery system where the experiment showed a reasonable agreement with the equations. Casano and Piva [32] also verified a good agreement for a thermoelectric generator system with one heat sink at the cold side and heat source on the hot side.

As for thermoelectric cooler, Chang et al. [33] tested a thermoelectric air-cooling system used for electronic devices and had a good agreement with the thermoelectric ideal equations. They conducted another experiment (using the same TEC module) in order to allow them to obtain the thermoelectric material properties and then used these properties in their main experiment. Huang et al. [34] did a similar work and also has a good agreement where their focus was on studying the effects of the thermal resistances of the system. These state-of-the-art studies are only a few of the many studies on the validation of the thermoelectric system which gave a good indication of the accuracy of the theoretical equations.

The majority of the work attempted on designing TEAC does not provide a clear method of how to optimize the TEAC system, especially the thermoelectric parameters. Moreover, a numbers of studies have been conducted either analytically or experimentally and only a few gather both the methods. Therefore, if an analytical study of the optimum design of the TEAC system is needed to be conducted, the accuracy of the design must also be investigated.

3.2 Objective

After understanding the basic concepts of thermoelectrics and finding the existence of room to improve TEAC design, the objective of this research is *to develop and experimentally validate the optimal design of automotive thermoelectric air conditioning system (TEAC).* To put it another way, the previous studies showed a number of designs but none of them could identify the optimum design regardless of how powerful the design was. The optimization of the thermoelectric parameters can be reached but usually by using a very complicated simulation system or by conducting costly experiments. Therefore, after the latest optimum design method presented by Lee [10], the aim of this work is focused on developing a simple technique to optimize the TEAC parameters. The optimal design theory provides a general method about optimizing the thermoelectric system and its application and validation can prove the depth of its correctness of the theoretical approach. In particular, there are many parameters that need to be discussed in order to investigate the availability of the optimum design of TEAC system, such as the thermal resistances of the heat exchanger attached to the thermoelectric device. However, for the thermoelectric cooler system, it is found that the electrical current and thermoelectric geometric ratio (or number of thermocouples) need to be optimized simultaneously. In order to reach that goal, the dimensional analysis theory is being modified and applied. Moreover, this design mainly deals with analytical calculations, and many factors may appear in the picture when the actual TEAC device is tested. Therefore, the experimental validation of the optimal design of the TEAC system is a necessity in order to determine the accuracy of the analytical work.

This objective is discussed and achieved through the following chapters where a brief description is shown below.

In Chapter 4, the main theories and analytical modeling, used to reach an accurate TEAC optimum design, are discussed. The first part of the chapter discusses the accuracy of the thermoelectric ideal equations when they are used to predict the performances. Then, the model of the optimum design of the TEAC system is discussed, addressing the dimensional analysis theory, along with heat sink optimization.

Chapter 5 focuses on how the experiments are setup in order to investigate the accuracy of the models presented in Chapter 4. Based on these models, two experiments have been conducted and the setup is discussed in this chapter. The first part of the chapter presents the experimental setup of a unit cell of the TEAC system while the other part presents the experimental setup that could simulate the whole TEAC system.

The results of the presented model and experiments are discussed in Chapter 6. The first part of the chapter discusses effective material properties of several thermoelectric module manufacturers and shows the accuracy of the method. After that, using the ideal equations and effective material properties, a design of air-to-liquid TEAC system found in the literature is studied in order to investigate the accuracy of the method. Then, this study is compared with a design that uses the optimum design theory. Finally, the results of the optimum air-to-air TEAC design and experiments are presented for both unit cell and whole system.

CHAPTER 4

TEAC MODELING

All information in this chapter is in reference to the methodologies explained in Ref. [35], [36], [12], and [37] with the author's contribution. The objective of this section is to study and optimize an analytical design of air-to-air TEAC. A proposed schematic is shown in Figure 4.1 and is discussed further in the upcoming sections. The proposed design is described as two layers of the thermoelectric module sandwiching cold air heat sink while two layers of hot air heat sinks are separately attached to the hot sides of the thermoelectric modules. The main focus of the analytical modeling is to simulate one unit cell of the optimum design of TEAC that can represent the whole system where that system is assumed to be divided into a number of equal unit cells. This is a straightforward method that is adopted from the dimensional analysis theory [10]. Moreover, the simulation of the whole TEAC system is discussed by combining the thermal isolation method along with the dimensional analysis method.

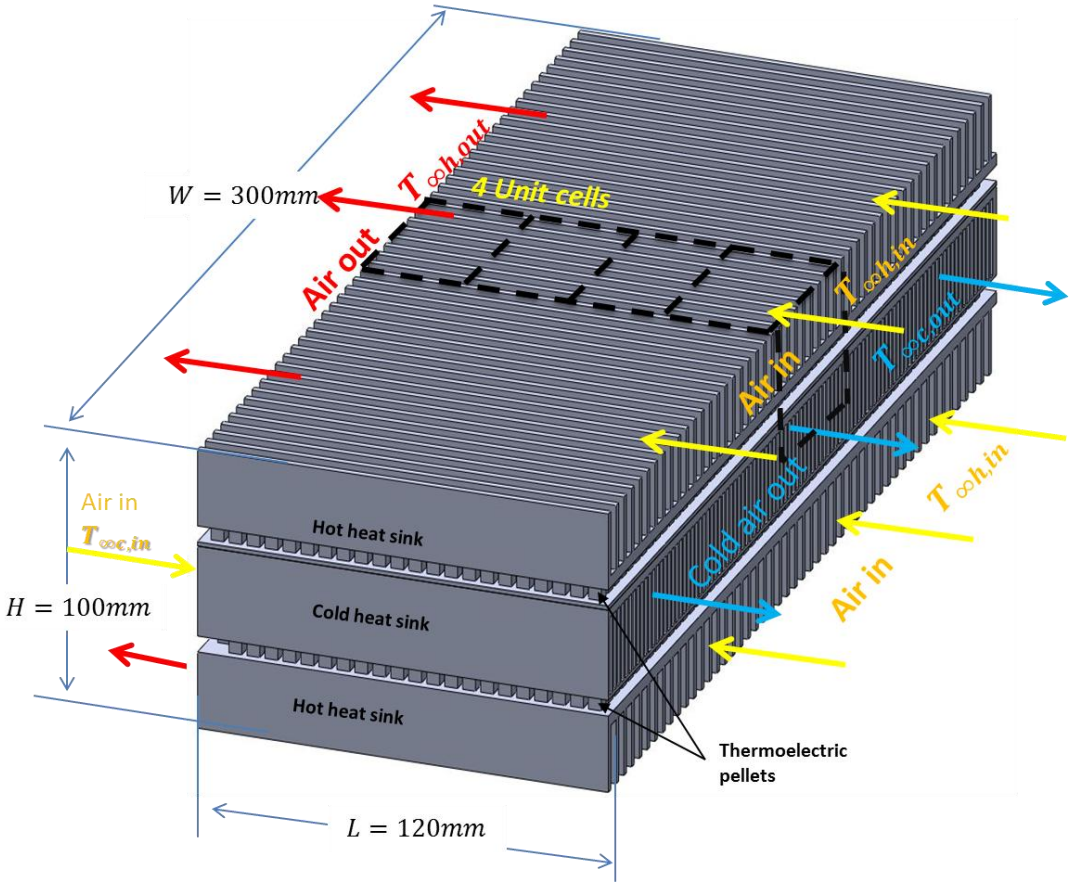

Figure 4.1. Schematic of air-to-liquid TEAC. [37]

4.1 Calculating the Effective Material Properties

The effective material properties are defined as the material properties that are extracted from the maximum parameters which are provided by the manufacturers. These properties are used instead of the intrinsic material properties in order to reduce the errors associated with the assumption of neglecting the contact resistances. The effective figure of merit is obtained from equation 2.52, which can be written as:

$$Z^* = \frac{2\Delta T_{max}}{(T_h - \Delta T_{max})^2} \qquad 4.1$$

The effective Seebeck coefficient is obtained using equations 2.51 and 2.54, which is as follows

$$\alpha^* = \frac{2\dot{Q}_{c,max}}{nI_{max}(T_h + \Delta T_{max})} \quad 4.2$$

the effective electrical resistivity can be obtained using equation 2.51, which is written as

$$\rho^* = \frac{\alpha^*(T_h - \Delta T_{max})A_e/L_e}{I_{max}} \quad 4.3$$

and finally the effective thermal conductivity is now obtained using equation 2.53, which is denoted as:

$$k^* = \frac{\alpha^{*2}}{\rho^* Z^*} \quad 4.4$$

These effective material properties include realistic effects such as contact resistances. Since the material properties are obtained for a p-type and n-type thermoelectric couple, the material properties of an element (either p-type or n-type) can be obtained by dividing by 2.

4.2 Use the Dimensional Analysis Method to Find the Thermoelectric Optimum Current and Geometric Ratio for a Unit Cell

The main goal of this section is to obtain the optimum design for the thermoelectric cooling system to maximize the COP by simultaneously optimizing the electrical current I and the thermocouple geometric ratio ($G_e = A_e/L_e$). Therefore, adopting the optimum design method using the dimensional analysis technique developed by Lee [10] can help us reach that goal. This method assumes that the electrical and thermal contact resistances in the TEC are neglected, the material properties are independent of temperature, the thermoelectric module is perfectly insulated, and the element dimensions p-type and n-type are identical. After that, the four basic heat balance equations (equation 4.5 to equation 4.8) can be converted into two non-

dimensional equations (equations 4.10 and 4.11). Figure 4.2 (a) and (b) show schematics of the unit cell of thermoelectric module with two heat sinks and one thermoelectric couple, respectively, where p and n types have similar pellet heights and cross-sectional areas.

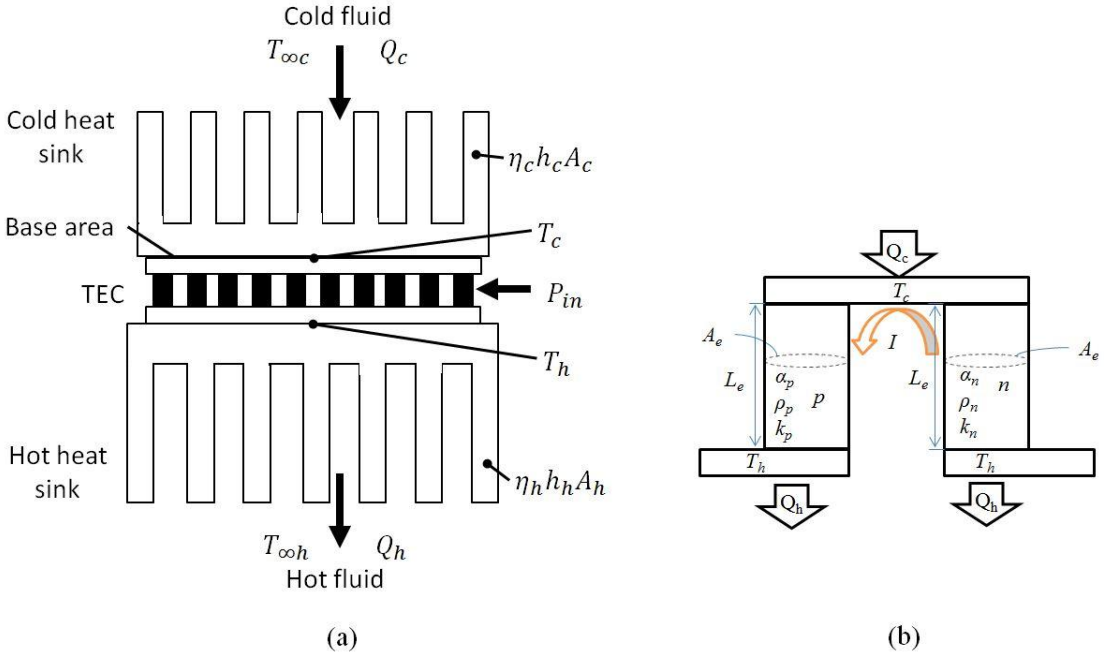

Figure 4.2. (a) thermoelectric cooler module (TEC) with two heat sinks, (b) schematic of thermoelectric couple. [35]

$$\dot{Q}_c = \eta_c h_c A_c (T_{\infty c} - T_c) \tag{4.5}$$

$$\dot{Q}_c = n\left[\alpha I T_c - \frac{1}{2} I^2 R + \frac{A_e}{L_e} k (T_c - T_h)\right] \tag{4.6}$$

$$\dot{Q}_h = n\left[\alpha I T_h + \frac{1}{2} I^2 R + \frac{A_e}{L_e} k (T_c - T_h)\right] \tag{4.7}$$

$$\dot{Q}_h = \eta_h h_h A_h (T_h - T_{\infty h}) \tag{4.8}$$

$$P_{in} = \dot{Q}_h - \dot{Q}_c \quad (4.9)$$

The thermal resistance of the heat sink can be expressed by the reciprocal of the convection conductance (i.e., $\eta_c h_c A_c$), where η_c is the fin efficiency, h_c is the convection coefficient, and A_c is the total surface area of the cold heat sink.

$$\frac{N_h(T_\infty^* - T_c^*)}{N_k} = N_I T_c^* - \frac{N_I^2}{2ZT_{\infty h}} + (T_c^* - T_h^*) \quad (4.10)$$

$$\frac{(T_h^* - 1)}{N_k} = N_I T_h^* - \frac{N_I^2}{2ZT_{\infty h}} + (T_c^* - T_h^*) \quad (4.11)$$

$ZT_{\infty h}$, N_h , N_k , and N_I are defined as the dimensionless figure of merit, convection ratio, the ratio of thermal conductance to the convection conductance, and dimensionless current, respectively.

$$ZT_{\infty h} = \frac{\alpha^2}{\rho k} T_{\infty h} \quad (4.12)$$

$$N_h = \frac{\eta_c h_c A_c}{\eta_h h_h A_h} \quad (4.13)$$

$$N_k = \frac{n(A_e k / L_e)}{\eta_h h_h A_h} \quad (4.14)$$

$$N_I = \frac{\alpha I}{A_e k / L_e} \quad (4.15)$$

T_c^*, T_h^* and T_∞^* are the dimensionless cold junction temperature, the dimensionless hot junction temperature, and the fluid temperature ratio, respectively, and are defined as

$$T_c^* = \frac{T_c}{T_{\infty h}} \quad (4.16)$$

$$T_h^* = \frac{T_h}{T_{\infty h}} \quad (4.17)$$

$$T_{\infty}^{*} = \frac{T_{\infty c}}{T_{\infty h}} \qquad 0.18$$

Then, it can be said that the dimensionless temperatures are functions of five independent dimensionless parameters as shown below

$$T_c^{*} = f(N_k, N_h, N_I, T_{\infty}^{*}, ZT_{\infty h}) \qquad 4.19$$

$$T_h^{*} = f(N_k, N_h, N_I, T_{\infty}^{*}, ZT_{\infty h}) \qquad 4.20$$

After that, the dimensionless cooling power (Q_c^{*}), heat rejection (Q_h^{*}), input power (P_{in}^{*}), and COP are defined as follows

$$\dot{Q}_c^{*} = \frac{\dot{Q}_c}{\eta_h h_h A_h T_{\infty h}} = N_h(T_{\infty}^{*} - T_c^{*}) \qquad 4.21$$

$$\dot{Q}_h^{*} = \frac{\dot{Q}_h}{\eta_h h_h A_h T_{\infty h}} = T_h^{*} - 1 \qquad 4.22$$

$$P_{in}^{*} = \frac{P_{in}}{\eta_h h_h A_{hT_{\infty h}}} = \dot{Q}_h^{*} - \dot{Q}_c^{*} \qquad 4.23$$

$$COP = \frac{\dot{Q}_c^{*}}{W_n^{*}} \qquad 4.24$$

Fixing $ZT_{\infty h}$, T_{∞}^{*} and N_h to be as inputs and optimize the dimensionless parameters N_k and N_I, equations 4.10 and 4.11 can be solved to give the maximum COP at a given input power.

4.3 Use the Thermal Isolation Method to Calculate the Local Ambient Temperatures

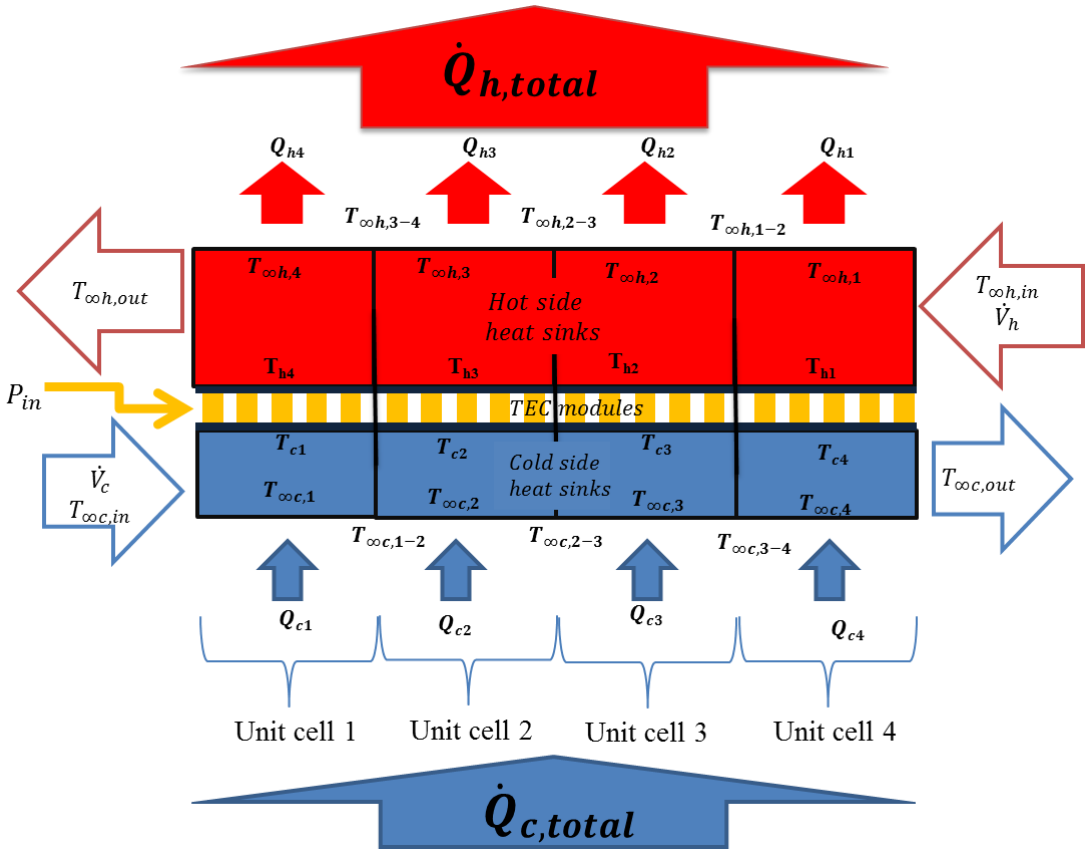

Figure 4.3. Schematic of four unit cells TEAC system. [37]

Figure 4.3 shows a schematic plot of the four-unit cell that is modeled in this section. This section focuses on simultaneously optimizing the input current and the geometric ratio of the element (or number of thermoelectric couples) for each unit that can provide the maximum possible COP_{total} at a given input electrical power using the optimum design method discussed earlier. In this method, dimensionless numbers are defined under the same assumptions assumed for the unit cell modeling. Moreover, the change of ambient temperature along the system is taken into consideration by adopting the thermal isolation method developed by Bell [11]. Combining and modifying the

optimal design and the thermal isolation methods allow us to analyze and optimize the whole TEAC system where the six basic heat balance equations (equation 4.25 to equation 4.30) around each unit cell can be converted into four non-dimensional equations (equation 4.33 to equation 4.36).

$$\begin{aligned}&\dot{Q}_{c,j}\\&= \dot{m}_c c_{p,c}\Bigg(-2T_{\infty c,j}\\&+\frac{4(j-1)(j-2)!}{(j-1)!}T_{\infty c,j-1}-\frac{4(j-1)(j-2)}{(j-1)!}T_{\infty c,j-2}\\&+\frac{4(j-1)(j-2)(j-3)}{(j-1)!}T_{\infty c,j-3}-2(-1)^j T_{\infty c,in}\Bigg)\end{aligned} \tag{4.25}$$

$$\dot{Q}_{c,j} = \eta_c h_c A_c\left(T_{\infty c,j} - T_{c,j}\right) \tag{4.26}$$

$$\dot{Q}_{c,j} = n_j\left[\alpha I T_{c,j} - \frac{1}{2}I_j^2\rho\frac{L_e}{A_e} + \frac{A_e}{L_e}k(T_{c,j} - T_{h,5-j})\right] \tag{4.27}$$

$$\dot{Q}_{h,5-j} = n_j\left[\alpha I T_{h,5-j} + \frac{1}{2}I_j^2\rho\frac{L_e}{A_e} + \frac{A_e}{L_e}k\left(T_{c,j} - T_{h,5-j}\right)\right] \tag{4.28}$$

$$\dot{Q}_{h,5-j} = \eta_h h_h A_h\left(T_{h,5-j} - T_{\infty h,5-j}\right) \tag{4.29}$$

$$\begin{aligned}&\dot{Q}_{h,5-j}\\&= \dot{m}_h c_{p,h}\Bigg(2T_{\infty h,5-j}\\&-\frac{4(4-j)(3-j)!}{(4-j)!}T_{\infty h,4-j}+\frac{4(4-j)(3-j)}{(4-j)!}T_{\infty h,3-j}\\&-\frac{4(4-j)(3-j)(2-j)}{(4-j)!}T_{\infty h,2-j}+2(-1)^{j+1}T_{\infty h,in}\Bigg)\end{aligned} \tag{4.30}$$

$$P_{in,j} = \dot{Q}_{h,5-j} - \dot{Q}_{c,j} \tag{4.31}$$

$$\dot{Q}_{c,total} = \dot{Q}_{c,1} + \dot{Q}_{c,2} + \dot{Q}_{c,3} + \dot{Q}_{c,4} \tag{4.32}$$

Where j represents the unit cell number ($j = 1, 2, 3, or\ 4$). Equations 4.25 and 4.30 represent the enthalpy flow, equations 4.26 and 4.29 represent the convective heat transfer from the heat sinks, and equations 4.27 and 4.28 represent the thermoelectric cooler ideal equations. $\dot{m}_c$ and $\dot{m}_h$ are the cold and hot air mass flow rates, $c_{p,c}$ and $c_{p,h}$ are the specific heat at the cold side and at the hot side respectively. These parameters as well as the heat sinks parameters are assumed to be constant for all four units. The average local ambient temperatures $T_{\infty c,j}$ and $T_{\infty h,5-j}$ can be obtained by averaging the inlet and exit temperatures of each unit (i.e., $T_{\infty c,1} = \left(T_{\infty c,in} + T_{\infty c,12}\right)/2$ and $T_{\infty h,4} = \left(T_{\infty h,34} + T_{\infty h,out}\right)/2$). Therefore, the dimensionless equations are

$$N_h\left(T^*_{\infty c,j} - T^*_{c,j}\right) = (\gamma_c + 1)\left[N_{kj}N_{Ij}T^*_{c,j} - \frac{N_{kj}N_{Ij}^2}{2ZT_{\infty h,in}} - N_{kj}\left(T^*_{h,5-j} - T^*_{c,j}\right)\right] \tag{4.33}$$

$$\begin{aligned} N_h\left(T^*_{\infty c,j} - T^*_{c,j}\right) &= (\gamma_c + 1)\varphi_c\Bigg(-2T^*_{\infty c,j} \\ &+ \frac{4(j-1)(j-2)!}{(j-1)!}T^*_{\infty c,j-1} - \frac{4(j-1)(j-2)}{(j-1)!}T^*_{\infty c,j-2} \\ &+ \frac{4(j-1)(j-2)(j-3)}{(j-1)!}T^*_{\infty c,j-3} - 2(-1)^j T^*_{\infty c,in}\Bigg) \end{aligned} \tag{4.34}$$

$$\begin{aligned} \left(T^*_{h,5-j} - T^*_{\infty h,5-j}\right) &= (\gamma_h + 1)\left[N_{kj}N_{Ij}T^*_{h,5-j} + \frac{N_{kj}N_{Ij}^2}{2ZT_{\infty h,in}} - N_{kj}\left(T^*_{h,5-j} - T^*_{c,j}\right)\right] \end{aligned} \tag{4.35}$$

$$\left(T^*_{h,5-j} - T^*_{\infty h,5-j}\right)$$

$$= (\gamma_h + 1)\varphi_h \left(2T^*_{\infty h,5-j} - \frac{4(4-j)(3-j)!}{(4-j)!} T^*_{\infty h,4-j} \right.$$

$$+ \frac{4(4-j)(3-j)}{(4-j)!} T^*_{\infty h,3-j} - \frac{4(4-j)(3-j)(2-j)}{(4-j)!} T^*_{\infty h,2-j} \qquad 4.36$$

$$\left. + 2(-1)^{j+1} \right)$$

γ_c and γ_h are the ratios of thermal resistances of the heat sink to the aluminum blocks that are individually sandwiched between the heat sink and the TE module and are discussed in the experimental setup chapter. φ_c and φ_h are the ratio of the enthalpy flow ($\dot{m}c_p$) to the heat sink thermal conductance for the cold and hot side, respectively.

$$\gamma_c = \frac{\eta_c h_c A_c}{k_{al} A_M / t_{al}} \qquad 4.37$$

$$\gamma_h = \frac{\eta_h h_h A_h}{k_{al} A_M / t_{al}} \qquad 4.38$$

$$\varphi_c = \frac{\dot{m}_c c_{p,c}}{\eta_h h_h A_h} \qquad 4.39$$

$$\varphi_h = \frac{\dot{m}_h c_{p,h}}{\eta_h h_h A_h} \qquad 4.40$$

where k_{al} is thermal conductivity of the aluminum block, A_M is the base or TEC module surface area, and t_{al} is the thickness of the aluminum block.

$T^*_{\infty c,in}$ is the ratio between the cold and hot inlet ambient temperature ($T^*_{\infty c,in} = T_{\infty c,in}/T_{\infty h,in}$). $T^*_{c,j}$, $T^*_{h,5-j}$, $T^*_{\infty c,j}$, and $T^*_{\infty h,5-j}$ are the dimensionless cold junction temperature, the dimensionless hot junction temperature, the cold fluid temperature ratio, and hot fluid temperature ratio of unit j, respectively.

$$T^*_{c,j} = \frac{T_{c,j}}{T_{\infty h,in}} \tag{4.41}$$

$$T^*_{h,5-j} = \frac{T_{h,5-j}}{T_{\infty h,in}} \tag{4.42}$$

$$T^*_{\infty c,j} = \frac{T_{\infty c,j}}{T_{\infty h,in}} \tag{4.43}$$

$$T^*_{\infty h,5-j} = \frac{T_{\infty h,5-j}}{T_{\infty h,in}} \tag{4.44}$$

The dimensionless junction temperatures and the fluid temperature ratios are then functions of eleven independent dimensionless parameters as

$$T^*_{c,j} = f(N_{k1}, N_{k2}, N_{k3}, N_{k4}, N_h, N_{I1}, N_{I2}, N_{I3}, N_{I4}, T^*_{\infty c,in}, ZT_{\infty h,in}) \tag{4.45}$$

$$T^*_{h,5-j} = f(N_{k1}, N_{k2}, N_{k3}, N_{k4}, N_h, N_{I1}, N_{I2}, N_{I3}, N_{I4}, T^*_{\infty c,in}, ZT_{\infty h,in}) \tag{4.46}$$

$$T^*_{\infty c,j} = f(N_{k1}, N_{k2}, N_{k3}, N_{k4}, N_h, N_{I1}, N_{I2}, N_{I3}, N_{I4}, T^*_{\infty c,in}, ZT_{\infty h,in}) \tag{4.47}$$

$$T^*_{\infty h,5-j} = f(N_{k1}, N_{k2}, N_{k3}, N_{k4}, N_h, N_{I1}, N_{I2}, N_{I3}, N_{I4}, T^*_{\infty c,in}, ZT_{\infty h,in}) \tag{4.48}$$

Setting $ZT_{\infty h,in}$, $T^{*}_{\infty c,in}$ and N_h to be the inputs, the dimensionless parameters N_{k1}, N_{k2}, N_{k3}, N_{k4}, N_{I1}, N_{I2}, N_{I3}, and N_{I4} can be optimized to solve equations 4.33 to 4.36 in order to maximize COP for given input power. The design requirements aim to have a total input power of 400W (or 20W for the four unit cell).

4.4 Optimizing the Heat Sink Parameters for a Unit Cell

Optimizing the heat sinks of the TEAC system is very critical in order to improve the performance. The same method discussed in section 2.4 is used to find the optimum fin spacing and thickness. The optimum fin spacing can simply be found by using equation 2.85 and then the fin thickness can be optimized to obtain the maximum heat transfer. On the other hand, finding the appropriate Nusselt number correlation Nu in order to obtain the heat transfer coefficient has a big impact on the heat sink performance. Therefore, the flow is considered as laminar channel flow where the Nusselt number correlation can be found [23].

4.5 Conclusion of the Chapter

Chapter 4 discussed the theories that are needed to obtain the optimum design of the TEAC system. The design is based on analytical models that use the ideal equations of thermoelectric system and heat sink. In order to improve the accuracy of the models, the effective material properties method is used, which is believed to minimize the errors associated with contact resistances and the assumption of using temperature independent properties. Furthermore, the validity of models is needed to be investigated experimentally as it is discussed in the next chapter.

CHAPTER 5

EXPERIMENTAL WORK

All information in this chapter is with respect to the methodologies explained in Ref. [36] and [37] with the author's contribution. The objective of this chapter is to clearly explain the two experimental setups that are constructed in order to investigate the accuracy of the optimal design models discussed in the last chapter. The goal of the first experiment (section 5.1) is to validate the optimum design model of the unit cell discussed in section 4.2 . Furthermore, the objective of the other experiment (section 5.2) is to validate the whole TEAC system modeling that was discussed in section 4.3.

5.1 Unit Cell Experimental Setup

In order to investigate the accuracy of a unit cell of air-to-air TEAC system, an experiment was needed to be built based on the inputs of the analytical model. Therefore, a system was built where a TEC module was sandwiched between two heat sinks.. The heat sinks and TEC modules are selected based on the optimized analytical design that was discussed in the previous chapter. Due to the limited availability of the dimensions of optimum heat sinks for the current work, closer commercial heat sinks were selected instead. Heat sinks ALPAH UB30-20B and ALPAH UB30-25B are used for the cold and hot sides, respectively. The overall experimental setup is shown in

Figure 5.1(a) and a detailed schematic of the test section is shown in Figure 5.1(b). Moreover, two aluminum blocks ($30 \times 30 \times 19.1\ mm^3$) are fabricated to be sandwiched between the TEC module and each of the heat sinks. Two parallel (5mm apart) K-type thermocouples were drilled to the center of the block where the average hot and cold blocks temperatures existed. Furthermore, two variable speed centrifugal blowers were used to drive the cold and hot airs where a temperature bath controller and a heater were used to control the inlet cold and hot air temperatures, respectively. A pitot tube connected to a manometer is fixed at the exit of the flow in order to determine the air speed of the hot and cold flow by measuring the dynamic pressure (the difference between the total pressure and static pressure). The blowers are adjusted to give a volumetric flow rate for cold and hot air of 3.21CFM and 6.1CFM, respectively. The average ambient cold and hot temperatures at the heat sinks $T_{\infty c}$ and $T_{\infty h}$, respectively, can be obtained by averaging the air inlet and exit temperatures for both cold and hot sides ($T_{\infty c,in}$, $T_{\infty c,out}$, $T_{\infty h,in}$, and $T_{\infty h,out}$) such that $T_{\infty c} = \frac{1}{2}\left(T_{\infty c,in} + T_{\infty c,out}\right)$ and $T_{\infty h} = \frac{1}{2}\left(T_{\infty h,in} + T_{\infty h,out}\right)$. These temperatures ($T_{\infty c,in}$, $T_{\infty c,out}$, $T_{\infty h,in}$, and $T_{\infty h,out}$) are measured by using E-type thermocouples installed at the air inlet and exit for both cold and hot air. On the other hand, the TEC input power is controlled by a variable DC power supply, which allows controlling the input voltage.

After simulating the model analytically, it is found that the unit cell input power $P_{in,UC}$ must be equal to 4.5W and the average ambient cold and hot temperatures are required to be at 21.6^{o}C and 33.6^{o}C, respectively. Therefore, the TEC supplied voltage, the cold air inlet temperature $T_{\infty c,in}$, and the hot air inlet temperature $T_{\infty h,in}$ are adjusted accordingly until the average ambient temperatures and the input power match the above

values where, $P_{in,UC} = I \times V_{in}$. After that, measurements were taken for each input voltage (with increment of 1V) after reaching a steady state condition until reaching maximum voltage V_{max} provided by the manufacturer as shown in flowchart in Figure 5.2.

The experiment targets to obtain the cold junction temperature T_c and the hot junction temperatures T_h. These junction temperatures can be obtained by extrapolating the two measured temperatures of each block (T_{c1}& T_{c2} for cold side and T_{h1} & T_{h2} for hot side) assuming linear change of the temperature across the aluminum block.

The test is conducted for three different TEC modules (module 1: Tellurex C2-30-1503, module 2: Tellurex C2-30-0904, and module 3: Marlow RC12-4) so that the effect of N_k on the TEAC performance can be investigated. All TEC modules share the same base area ($30 \times 30\ mm^2$), but a different number of couples and/or element geometric ratio, G_e.

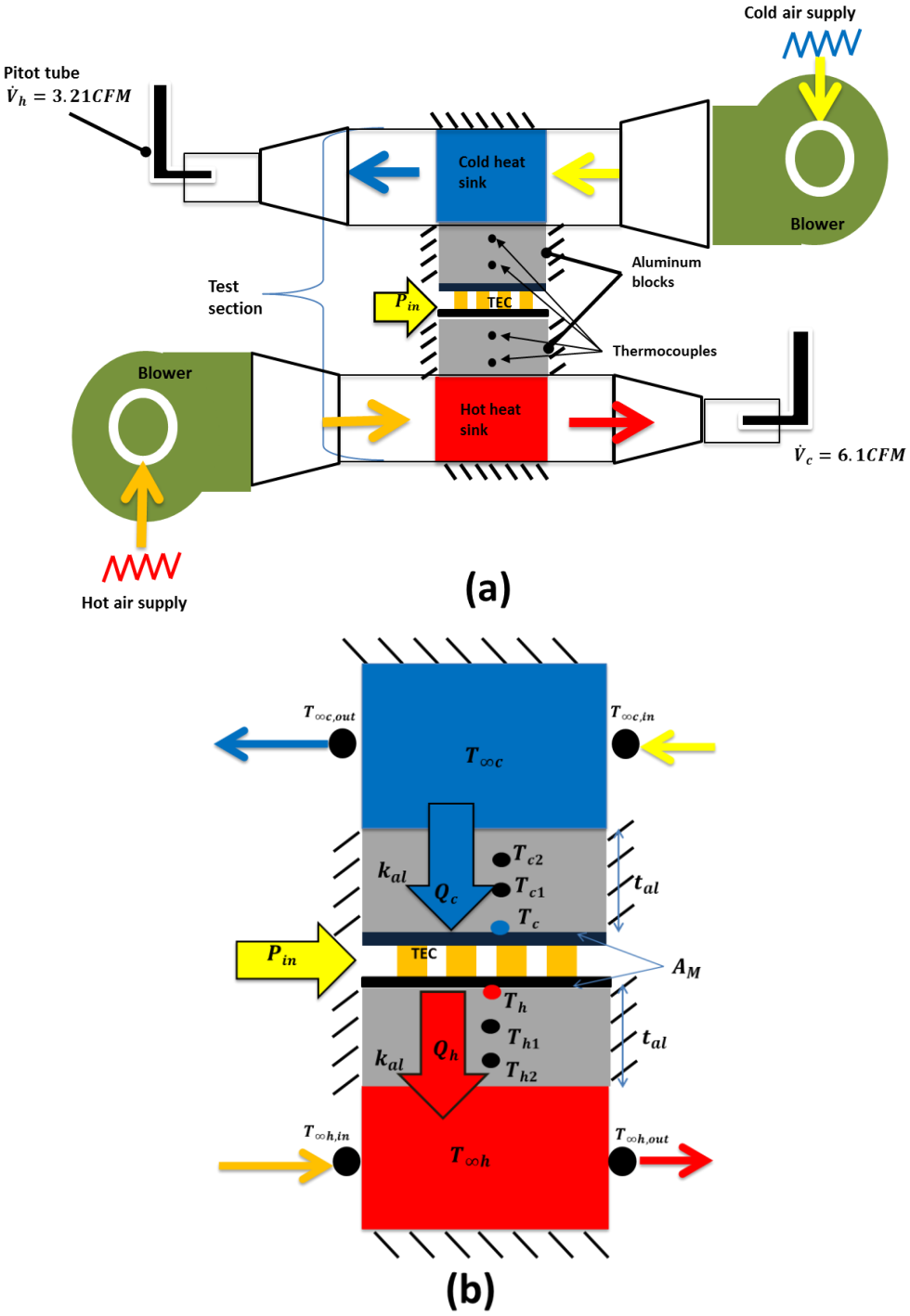

Figure 5.1. (a) Experimental setup of one unit cell of TEAC system, (b) test section. [36]

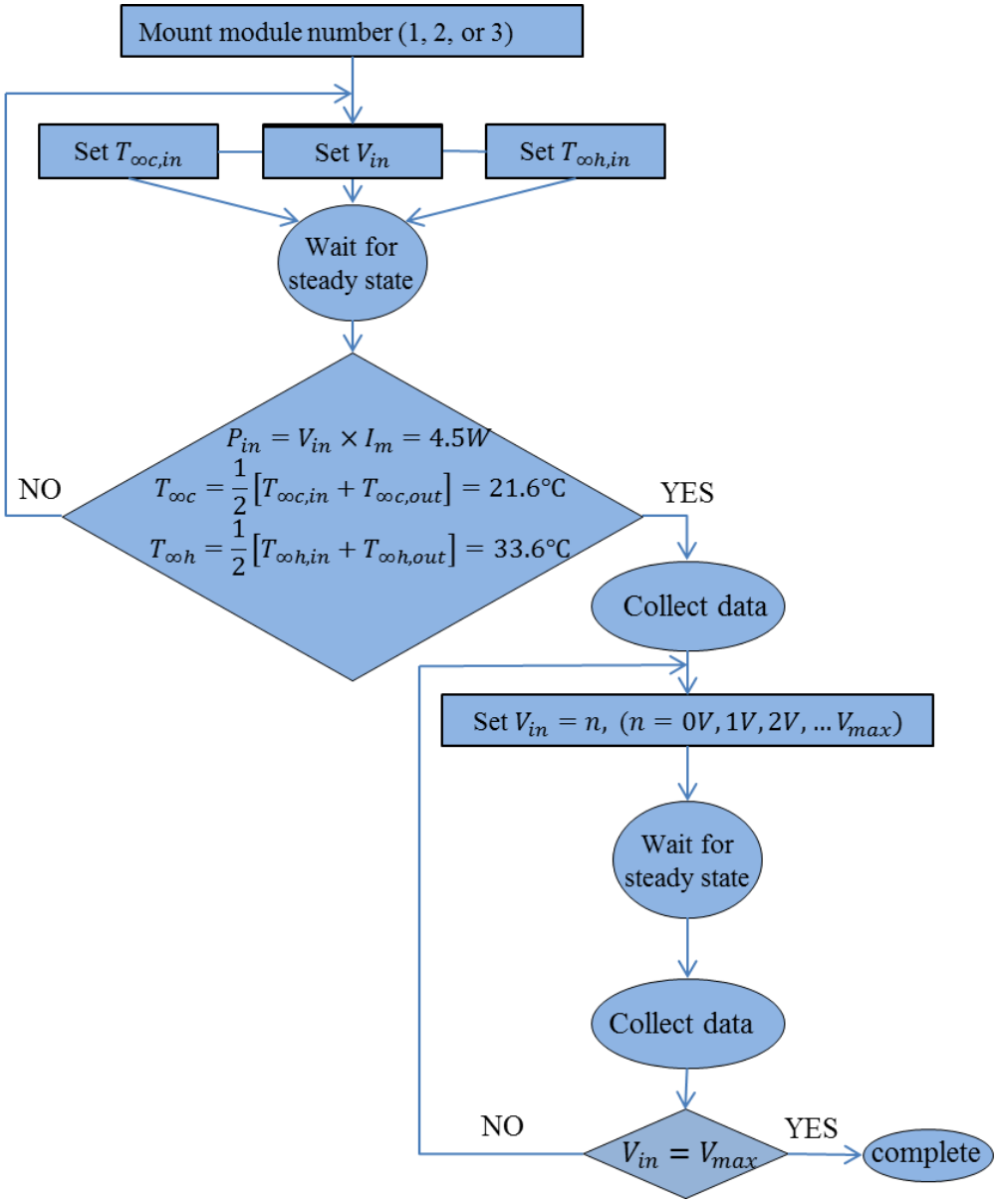

Figure 5.2. Flowchart of the experimental procedure. [36]

5.2 Whole System Experimental Setup

This experiment is designed to validate the proposed analytical design shown in section 4.3. The experimental setup is very similar to the one discussed in the previous section with the consideration of having four TEC unit cells connected in series.

Therefore, four identical commercial TEC modules are sandwiched between four heat sinks each for the hot side and the cold side.. The selection of the TEC modules and the heat sinks are based on commercially available items that have the closest dimensions to the one obtained from the optimized analytical design. As a result, four TEC modules TE-127-1.0-2.5 (made by TETECHNOLOGY, INC) in addition to the four heat sinks of ALPAH UB30-20B and four of ALPAH UB30-25B were used for the cold and hot sides, respectively, for this experiment. A photograph of this experiment and detailed schematic of the experimental setup is shown in Figure 5.3 (a) and (b), respectively.

The aluminum blocks are also sandwiched between each TEC module and its related heat sinks in order to measure the TEC junction temperatures as discussed earlier. Moreover, in order to minimize the thermal conduction between the unit cells, low thermal conductivity wooden plates are installed between the unit cells. As for the ambient cold and hot air, two variable speed centrifugal blowers (AMETEK 119350-51 BLOWER, 76MM, 24VDC) are used to pump the air where each blower is connected to a TEC system in order to control the inlet cold and hot air temperatures. These blowers are selected due to their high pumping ability so that back pressure can be avoided. The blowers are set to have volume flow rates of 3 CFM and 6 CFM for cold ($\dot{V}_c$) and hot ($\dot{V}_h$) air, respectively. These flow rates are obtained with same technique used in the previous section. As for the air temperatures, K-type thermocouples are installed at the air inlet, exit, and between each unit for the cold and hot sides so that the local ambient air temperatures at each unit can be averaged. Furthermore, the TEC modules are connected in series where variable DC power supply is used to supply and control the input voltage.

The inputs for the system are obtained from the analytical model where the total supplied power to the TECs is 20W ($P_{in,4units} = I_m \times V_{in,total} = 20W$) and the inlet ambient cold ($T_{\infty c,in}$) and hot ($T_{\infty h,in}$) temperatures should be maintained at 30^{o}C. Then, under steady state conditions the readings are recorded for each input voltage (with increment of 4V) until the maximum voltage per module (provided by the manufacturer) is reached as shown in flowchart in Figure 5.4.

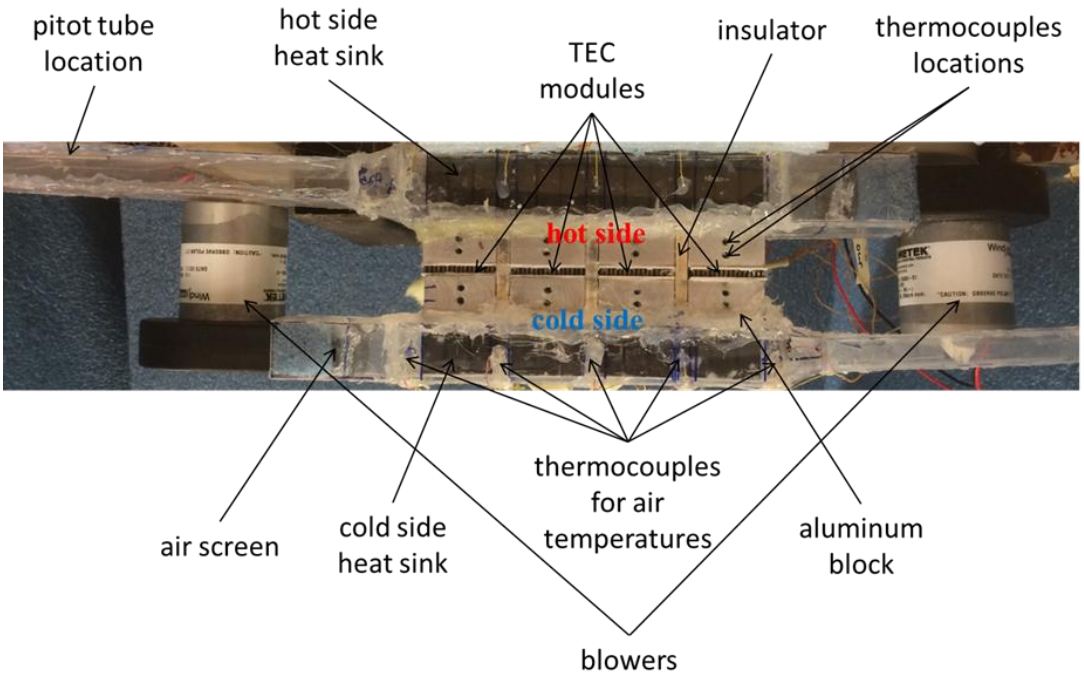

(a)

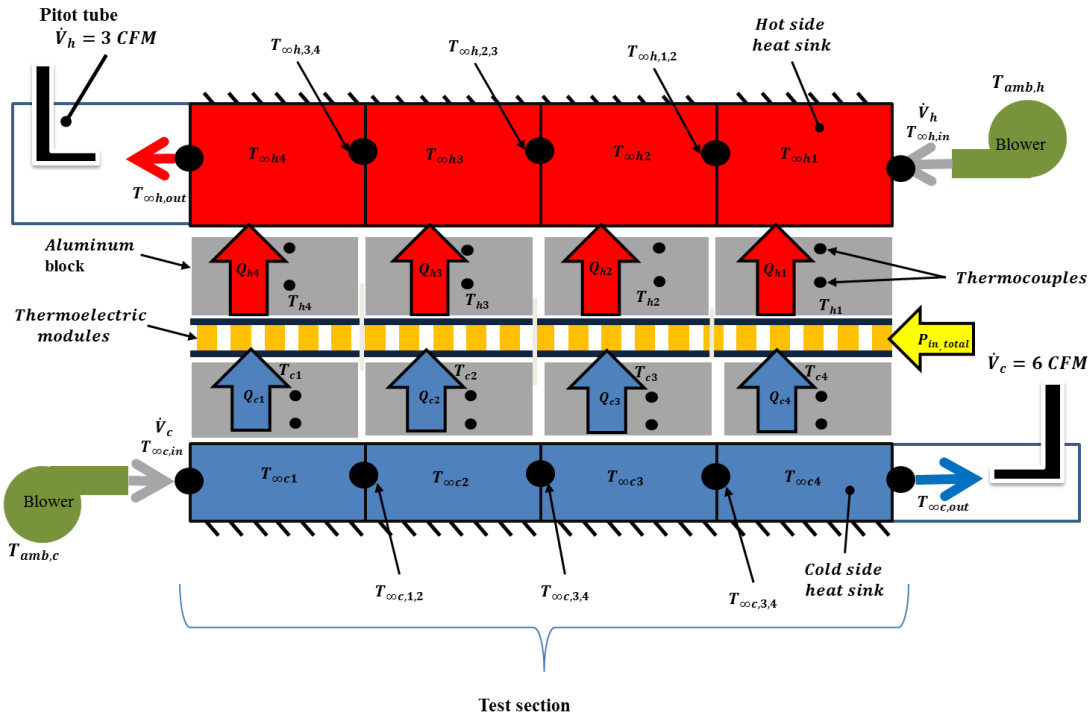

(b)

Figure 5.3. (a) Photograph of the test stand and (b) Schematic of the experimental setup of the four unit cells. [37]

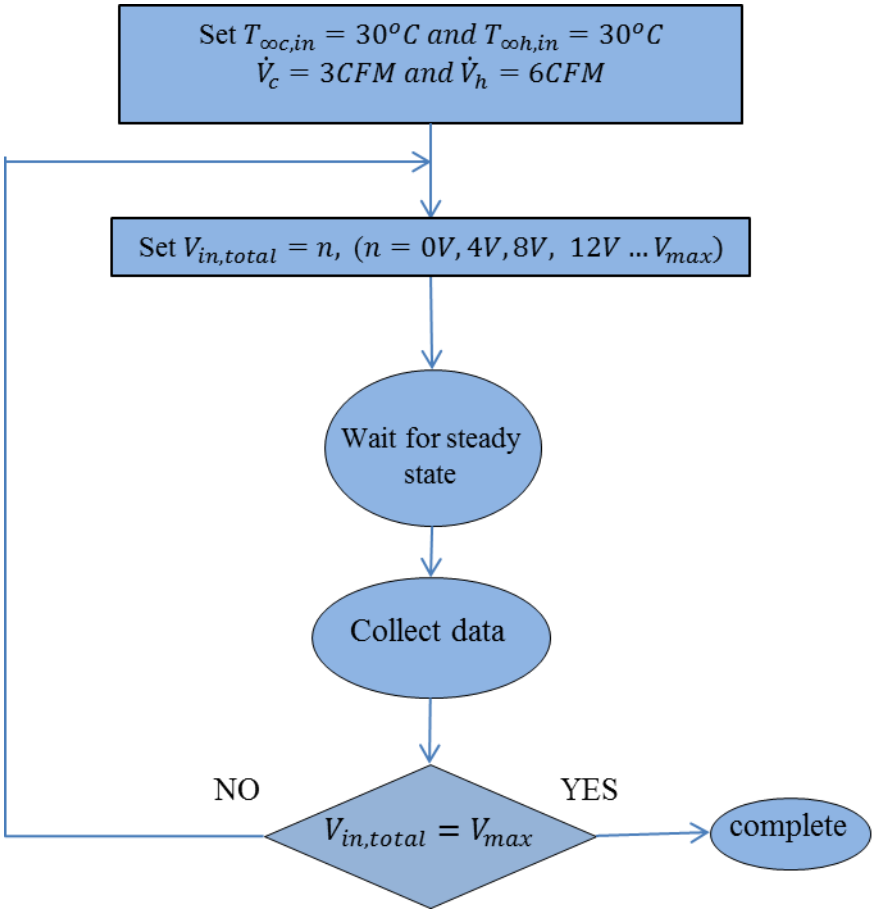

Figure 5.4. Flowchart of the experimental procedure for four TEAC units. [37]

CHAPTER 6

RESULTS AND DISCUSSIONS

All information in this chapter is with respect to the methodologies explained in Ref. [35], [36], [12], and [37] with the author's contribution. The chapter begins with addressing the results of the effective material properties of five different commercial products. After that, an existing design of air-to-liquid TEAC, found in the literature, is validated using the ideal equations and then compared with another design that uses the dimensional analysis where they both have the same inputs. Next, the results of the optimum design of air-to-air TEAC of unit cell are presented and compared with the unit cell experiment discussed in section 5.1. Finally, discussion and experimental validation of the optimum design of the whole TEAC system is addressed in the last section of this chapter.

6.1 Effective Material Properties

Consider a commercial thermoelectric cooler module (Laird CP10-127-05) where the intrinsic material properties of bismuth telluride (α, ρ, and k) are provided [38]. Moreover, from the provided manufacturer data sheet, the maximum parameters ($\Delta T_{max}, I_{max}, \dot{Q}_{max}, and\ V_{max}$) are believed to be obtained experimentally [39]. Using maximum parameters ($\Delta T_{max}, I_{max},\ and\ \dot{Q}_{max}$) and equations 4.1 through 4.4, the effective material properties α^*, ρ^*, Z^*, and k^*can be obtained. Table 6.1 shows a

comparison between the intrinsic material properties found by Laird [38] and calculated effective material properties using the maximum parameters. Note that the intrinsic figure of merit of 0.803 is slightly larger than the effective figure of merit of 0.744, which is reasonable when considering the contact resistances partially imposed on the effective material properties. More importantly, the three effective maximum parameters ΔT_{max}, I_{max}, and $\dot{Q}_{max}$ are identical to the manufacturer's maximum parameters, which are the results from the combinations chosen in calculating the effective material properties. Note that V_{max} and R show some discrepancy, as expected. The table also shows the effective material properties for the analyzed and tested modules for the current work (modules Tellurex C2-30-1503, Tellurex C2-30-0904, Marlow RC12-4, and TE-127-1.0-2.5).

It is understood that the selection of the present combination causes the errors between the ideal equation and reality to lie within both the maximum voltage V_{max} and the total resistance R. This method seems more practical wherein the errors do not lie within the maximum cooling power $\dot{Q}_{max}$ (which is the most important parameter). Figure 6.1 (a), (b), and (c) show the comparison between the manufacturer performance curves and the performance curves using the effective material properties. The cooling power comparison shows a very good agreement while the discrepancy appears in the voltage and the COP.

Table 6.1

The Calculated Effective Material Properties

		Intrinsic Material Properties	**Effective Material Properties**				
Description	**Symbols**	**Laird Module (CP10-127-05)** [38] [39]	**Laird Module (CP10-127-05)** [12]	**C2-30-1503**	**C2-30-0904**	**RC12-4**	**TE-127-1.0-2** [37]
Hot junction temperature	$T_h\ (K)$	298	298	323	323	323	323
# of thermocouples	n	127	127	127	71	127	127
Seebeck coefficient	$\alpha\ (\mu V/K)$	202.17	189.2	210.8	209.3	208.98	207.13
Electrical resistivity	$\rho\ (\Omega cm)$	1.01×10^{-3}	0.9×10^{-3}	1.09×10^{-3}	1.0×10^{-3}	1.2×10^{-3}	1.07×10^{-3}
Thermal conductivity	$k\ (W/cmK)$	1.51×10^{-2}	1.6×10^{-2}	0.016	0.018	0.015	0.015
Dimensionless figure of merit	ZT_h	0.803	0.744	0.804	0.804	0.77	0.857
Thermoelement cross-sectional area	$A_e\ (mm^2)$	1.0	1.0	1.21	1.69	1.0	1.0
Thermoelement length	$L_e\ (mm)$	1.25	1.25	1.66	2.0	1.17	2.5
Thermoelement geometric ratio	$G_e = A_e/L_e\ (cm)$	0.08	0.08	0.073	0.085	0.085	0.04
Module dimension	$W_M \times L_M \times H_M\ (mm^3)$	30 × 30 × 3.2	30 × 30 × 3.2	30×30×3.7	30×30×4.2	30×30×3.4	30×30×4.8
Maximum temperature difference	$\Delta T_{max}\ (°C)$	67	67	76	76	74	79
Maximum current	$I_{max}\ (A)$	3.9	3.9	3.5	4.4	3.7	1.9
Maximum cooling power	$\dot{Q}_{c,max}\ (W)$	34.3	34.3	37.4	26.1	39	20.1
Maximum voltage	$V_{max}\ (V)$	14.4	14.37	17.36	9.7	16.4	17.6
Module resistance	$R\ (\Omega)$	3.36	2.86	3.781	1.67	3.57	6.761

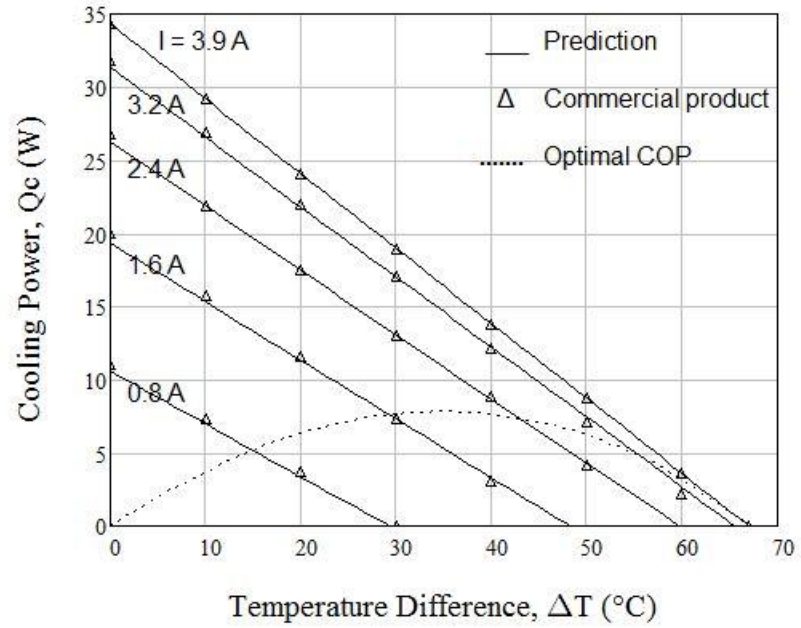
I = 3.9 A
3.2 A
2.4 A
1.6 A
0.8 A
Prediction
Commercial product
Optimal COP
Cooling Power, Qc (W)
Temperature Difference, ΔT (°C)
0
5
10
15
20
25
30
35
0
10
20
30
40
50
60
70

(a)

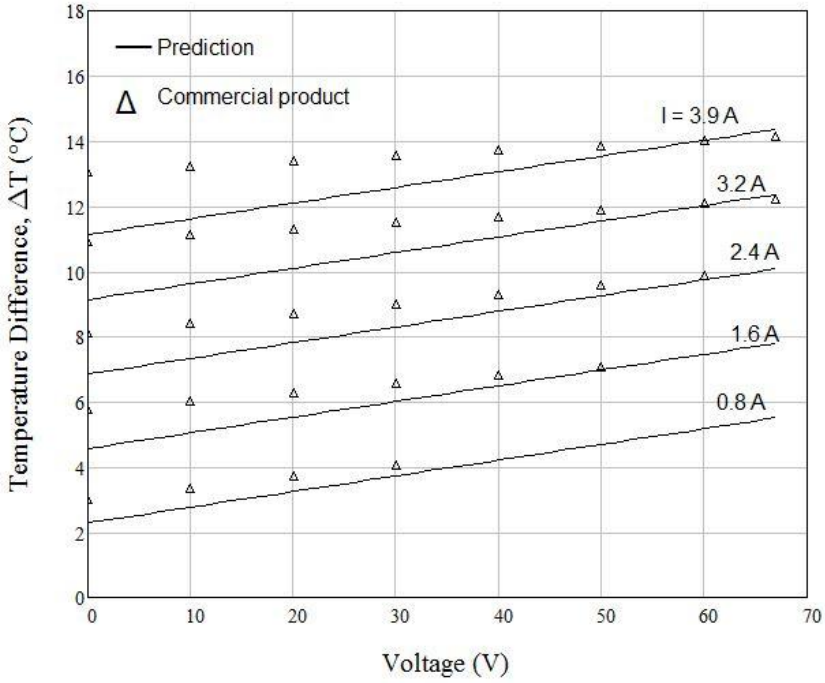
Prediction
Commercial product
I = 3.9 A
3.2 A
2.4 A
1.6 A
0.8 A
Temperature Difference, ΔT (°C)
Voltage (V)
0
2
4
6
8
10
12
14
16
18
0
10
20
30
40
50
60
70

(b)

Figure 6.1—Continued

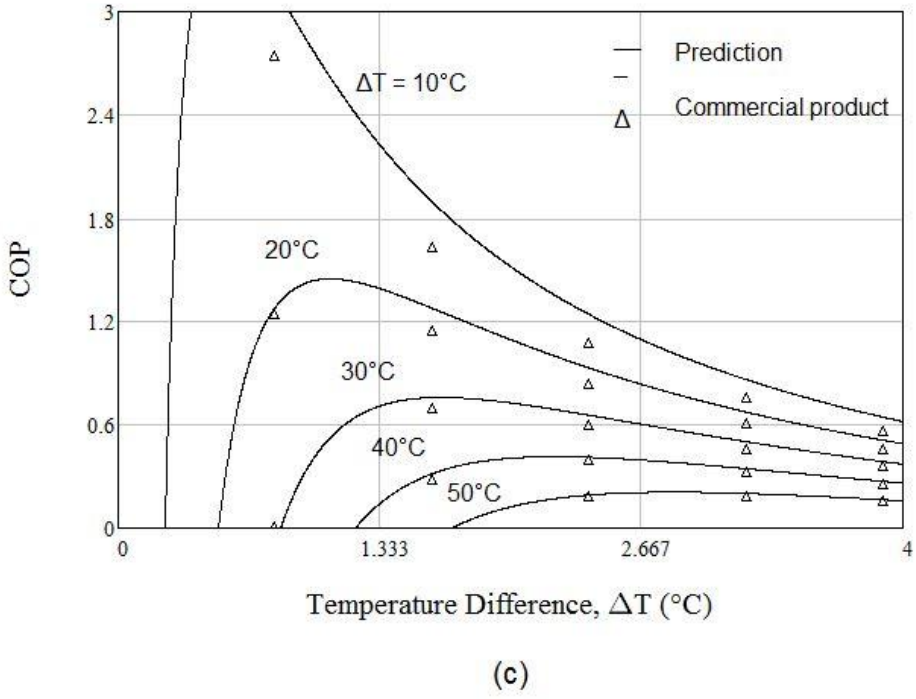

Figure 6.1. (a) Cooling power versus ΔT, (b) Voltage versus ΔT, as a function of current, and (c) COP versus current as a function of ΔT. The original performance data (triangles) of the commercial module (Laird CP10-127-05) are compared to the prediction (solid line). [12]

6.2 Air-to-liquid TEAC Study

A study of available air-to-liquid TEAC design developed by Gentherm [9] has been regenerated and compared with the optimum design method (using the dimensional analysis). This study is approached by applying the thermoelectric cooler basic equations and using several assumptions so that Gentherm performance curve can be regenerated (referred to a predicted data). In order to do so, the input parameters must first be identified. Moreover, several assumptions had to be made since not all of the needed input parameters were readily available. The assumptions can be validated if the results from the present analytical model are comparable with the results from Gentherm. After

that, these assumptions along with inputs parameters can be used in the optimum design model.

6.2.1 Gentherm Study

The objective of this particular section is to regenerate the performance curve provided by Gentherm [9] using the basic ideal equations and readily available data. Also, several assumptions have been made since some information is not provided. The Gentherm air-to-liquid TEAC system contains two layers of thermoelectric modules sandwiching a double-pass liquid heat exchanger and having air heat sinks attached to the cold side of each layer of thermoelectric modules in a cross-flow orientation with the liquid heat exchanger. Therefore, the dissipated heat from the hot side of thermoelectrics is absorbed by the liquid, where the liquid is being cooled independently at a separate heat exchanger. The ambient air is being cooled when passing over the heat sinks where the cold side of thermoelectric modules absorbs the air temperature before entering the cabin. The total dimensions of the TEAC system are $300mm \times 120mm \times 50mm$ ($W \times L \times H$). Moreover, the air flow rate is 60 CFM and the cold side temperature difference between the inlet and exit of cooling air, $\Delta T_{cooling}$, is 16.8°C at input power P_{in} of 400 W and COP of 1.3. Figure 6.2 (a) shows a schematic drawing of the whole Gentherm air-to-liquid TEAC system.

As mentioned earlier, not all of the needed input parameters were readily available, so several assumptions had to be made in order to regenerate Gentherm's performance curve. These assumptions are: the inlet ambient cold temperature $T_{\infty c,in}$ is 30^{o}C, the inlet hot liquid temperature $T_{\infty h,in}$ is 30°C, linear changes of the temperatures along the TEAC system for the cold and hot fluids, the liquid (working fluid) is 50%

ethylene glycol, the liquid flow rate V_h is 7 liters per minute, the materials for the heat sink and heat exchanger are aluminum, the heat sink fin profile length b_c is 15 mm, fin thickness t_c is 0.23mm, number of fins n_c is 437, and the heat exchanger height b_h is 5 mm. As for the thermoelectric module, the geometry factor G_e and the total number of couples n for the system are obtained to be approximately 0.365 cm and 880, respectively. Also, all calculations are made under the assumption of steady state conditions and by using the effective material properties.

The design is modeled by simulating a unit cell of $30\ mm\ x\ 30\ mm$ base area, as shown in Figure 6.2 (b), instead of analyzing the entire system where the power density of the full scale (cooling power divided by total base area, $A_b = L \times W$) is used to find the unit cell cooling power and input power at the same COP. The provided parameters by Gentherm are $P_{in} = 400W$ and $COP = 1.3$ which relates to $Q_c = P_{in} \times COP = 520W$. As a result, the unit cell cooling power $Q_{c,UC}$ is equal to 6.5W, which is obtained by the area ratio between the unit cell and Gentherm TEAC base areas ($Q_{c,UC} = \frac{1}{2} Q_c \times \frac{A_{UC}}{A_b}$). A factor of $\frac{1}{2}$ was used because the whole system has two layers of thermoelectric modules. The local ambient cold air temperature at the unit cell $T_{\infty c}$ is obtained by averaging the inlet and outlet cold air temperatures assuming linear change in the temperature of the unit cell. Similarly, local ambient hot liquid temperature $T_{\infty h}$ at the unit cell is obtained by averaging the inlet and outlet hot liquid temperatures where the exit hot liquid temperature $T_{\infty h,out}$ is calculated from the enthalpy flow equation $\left(Q_h = V_h \rho_h c_{p,h}\left(T_{\infty h,out} - T_{\infty h,in}\right)\right)$. On the other hand, the heat transfer coefficient of the heat sink is obtained from the Nusselt number correlation found in [22]. Finally, the junction

temperatures of the unit cell can be calculated by using the four basic equations (equations 2.78 to 2.81) where the input current I is varied until Q_c and Q_h match the values of Gentherm design. The obtained results are compared with the original data from Gentherm as shown in Table 6.2. This table compares two particular experimental data points (at input powers of 400W and 300W) of Gentherm with the prediction model that uses ideal equations. Moreover, Figure 6.3 compares Gentherm performance curve and the predicted work for COP vs. input power. It can be seen from the figure that the second experimental data point of Gentherm ($COP = 1.3$ at $P_{in} = 400W$) matches with the prediction since this data is the reference point for the predicted calculations. Furthermore, it can be seen from the figure that the prediction's trend under a wide range of input power shows fair agreement with the data from Gentherm. As a result, this prediction based on Gentherm's data can be considered as a new basis for comparison with the optimum design.

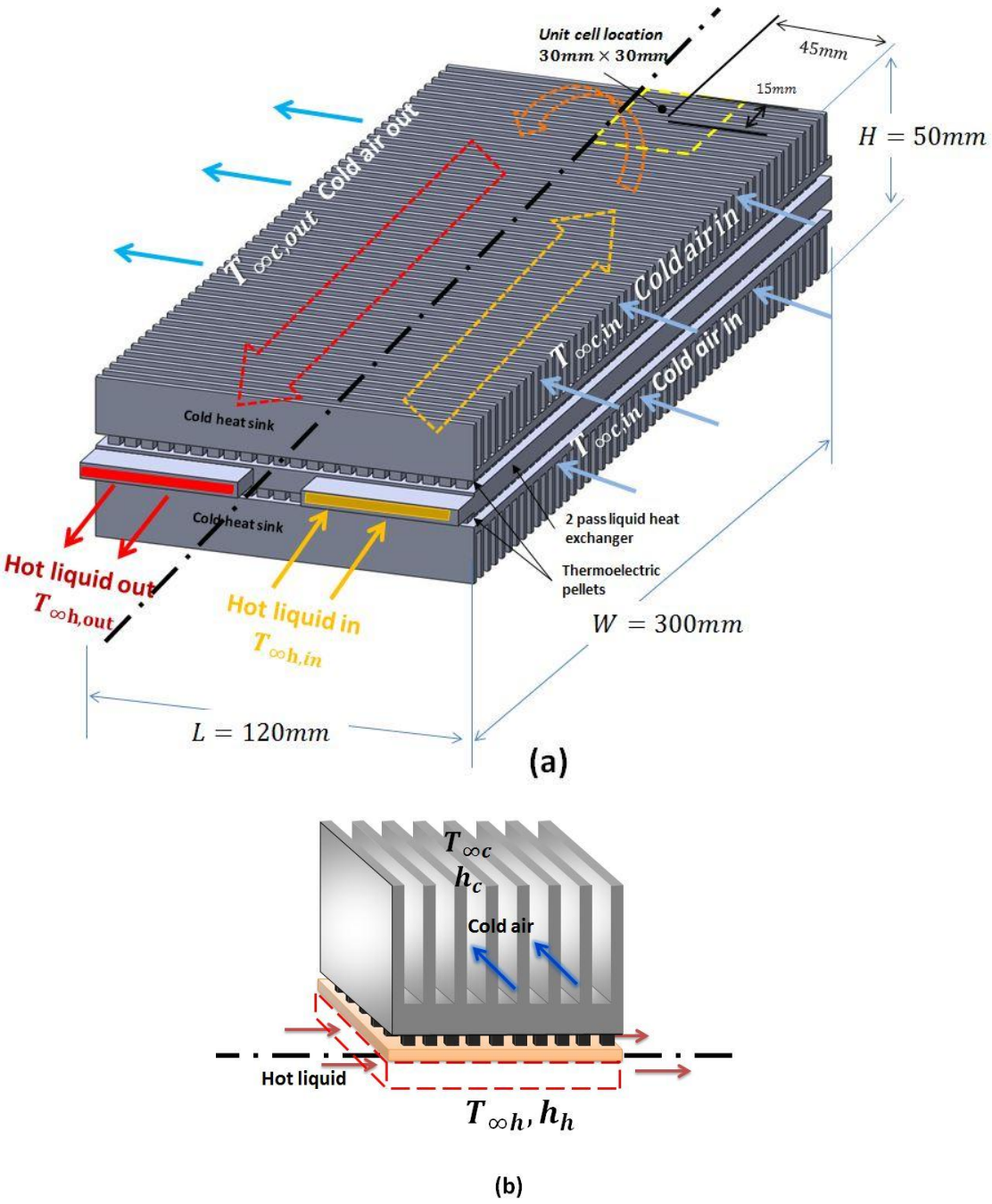

Figure 6.2. (a) Schematic diagram of Gentherm air-to-liquid TEAC, (b) Unit cell schematic. [35]

Table 6.2

Comparison between Gentherm Design and the Present Prediction for Two Input Powers of 400W and 300W [35]

Parameters	**Gentherm**	**Prediction**	**Gentherm**	**Prediction**
P_{in} (W)	400	409.59	300	287.67
I (A)	NA	9.1	NA	7.59
T_c (^{o}C)	NA	18.33	NA	19.05
T_h (^{o}C)	NA	34.93	NA	33.97
$\Delta T_{cooling}$ (°C)	16.8	16.8	15.0	15.0
COP	1.3	1.3	1.6	1.6
Q_c (W)	520	533.02	480	460.13
PD (W/cm^2)	0.722	0.74	0.67	0.64

H = 50mm, W = 300mm, L =120mm, V_c = 60CFM
Assumptions: V_h = 7.0 L/min, $T_{\infty c,in}$ = 30.0^{o}C, $T_{\infty h,in}$ = 30.0^{o}C, $T_{\infty c}$ = *23.6^{o}C*, $T_{\infty h}$ = *31.09^{o}C*, t_c = 0.23mm, n_c = 437, b_c = 15 mm × 2, b_h = 5 mm, A_{UC} = 9.0 cm^2, n = 880, G_e = 0.365 cm, $\alpha_p = -\alpha_n$ = 189.2μV/K, $\rho_p = \rho_n$ = 0.9x10^{-3} Ωcm, $k_p = k_n$ = 1.6x10^{-2} W/cmK, $ZT_{\infty h}$ = 0.756

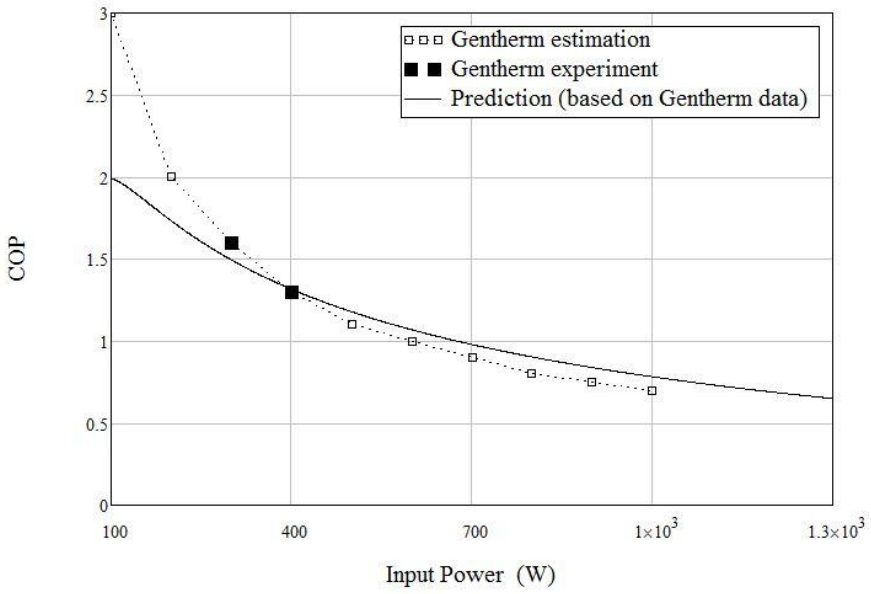

Figure 6.3. COP vs. Input Power for Gentherm work and present prediction [35]

6.2.2 Air-to-Liquid Optimum Design

The optimum design method discussed in section 4.2 requires us to have $ZT_{\infty h}$, T_{∞}^{*}, and N_h as inputs so that the non-dimensional parameters (N_I, N_k, Q_c^{*}, COP, T_c^{*}, T_h^{*}, and P_{in}^{*}) can be obtained. Then, the performance of the unit cell TEAC system can be obtained from these non-dimensional parameters using equations 4.21 to 4.24. The goal is to simultaneously optimize N_I and N_k in order to obtain the optimum input current and optimum thermoelectric geometric ratio. Therefore, the same parameters used in the previous section (unit cell ambient temperatures $T_{\infty c}$ and $T_{\infty h}$, thermoelectric figure of merit, and heat sink and heat exchanger) are applied for the optimum design modeling. As a result, $ZT_{\infty h}$, T_{∞}^{*}, and N_h are set to be the input parameters to solve for the dimensionless junction temperatures (T_c^{*} and T_h^{*}). After that, N_I and N_k can be optimized to give the maximum COP at a given input power.

Figure 6.4 shows cooling power Q_c, input power P_{in}, and COP vs. (a) dimensionless current, N_I, and (b) the ratio of thermal conductance to the convection conductance, N_k. It can be seen from the figure that the optimum current for maximum cooling power is different from the optimum current at maximum COP. However, the proposed work is designed to have the maximum COP at input power of 400W. Table 6.3 shows a comparison between the prediction based on Gentherm data and the current optimum design for air-to-liquid TEAC. For the same input power, the optimum design shows a significant improvement in COP and cooling power since the electrical current and geometry factor are optimized simultaneously.

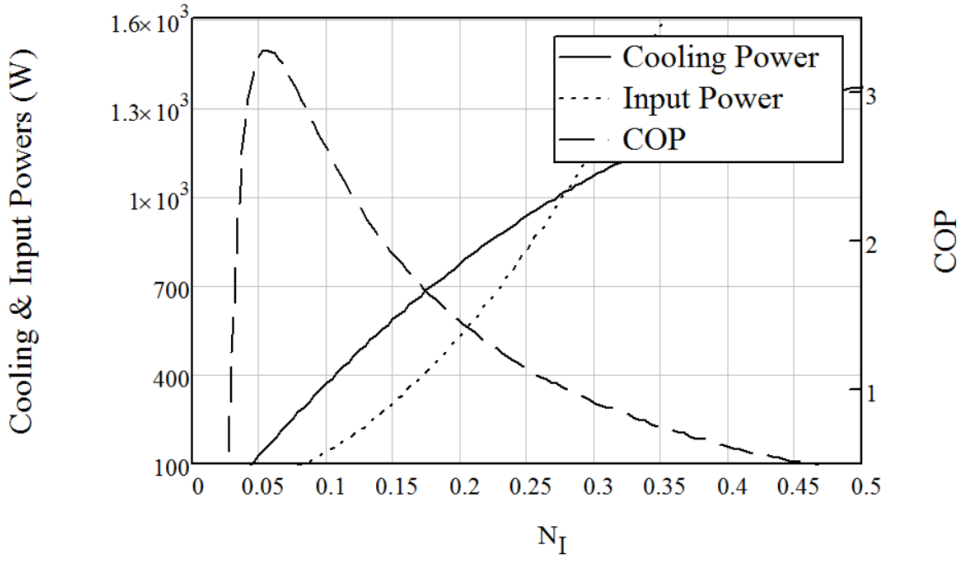

(a)

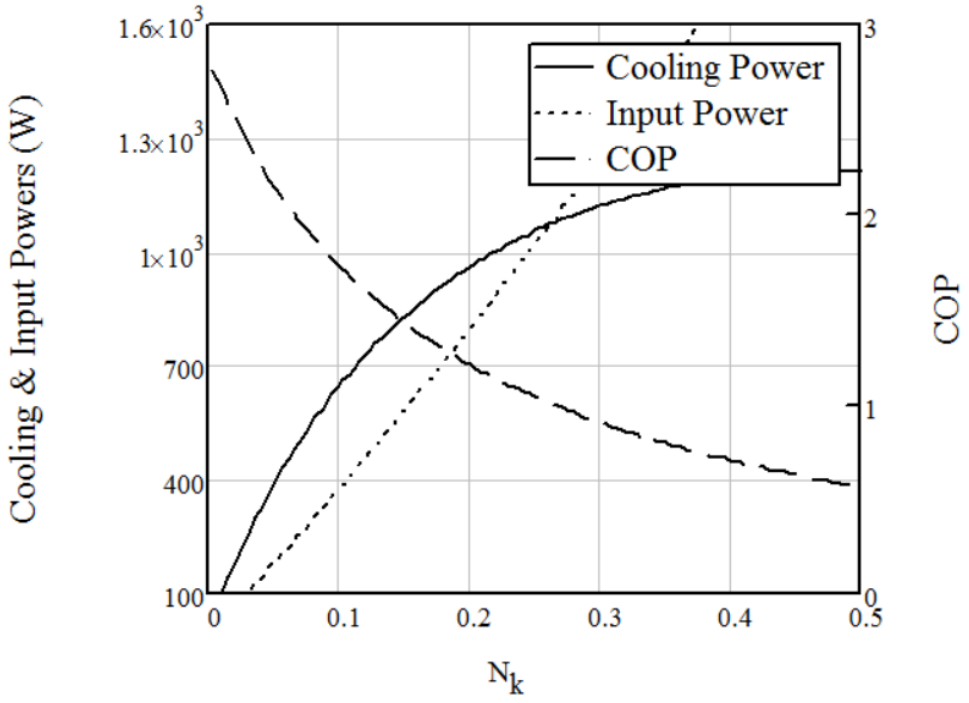

(b)

Figure 6.4. Cooling power, input power, and COP vs. (a) dimensionless current, N_I and (b) the ratio of thermal conductance to the convection conductance, $\mathbf{N_k}$.

Table 6.3

Comparison between Gentherm Predicted Design and Optimum Design [35]

Parameter	Prediction (Gentherm base)	Optimum Design
T_c (^oC)	18.33	16.79
T_h (^oC)	34.93	35.35
I (A)	9.1	13.66
G_e (cm)	0.365	0.93
P_{in} (W)	409.59	401.22
COP	1.3	1.68
Q_c (W)	533.02	672.38
PD (W/cm^2)	0.74	0.934

V_c = 60.0 CFM, V_h = 7.0 L/min, $T_{\infty c}$ = 23.6^oC, $T_{\infty h}$ = 31.09^oC, t_c = 0.23mm, z_c = 0.46mm, b_c = 15 mm x 2, b_h = 5 mm, h_c = 35.78W/m^2K, h_h = 2922W/m^2K, $\eta_c h_c A_c$ = 1.28W/K, $\eta_h h_h A_h = 3.07W/K$, $N_h = 0.417$, A_{UC} = 9.0 cm^2, n = 880, $ZT_{\infty h}$ = 0.756,

In addition to the optimum design, the dimensionless method has the advantage of predicting the TEAC optimum design for different figure of merits $ZT_{\infty h}$. Once $ZT_{\infty h}$ is increased, the optimum current and geometric factor will be changed. Table 6.4 shows the performances of air-to-liquid TEAC for different values of $ZT_{\infty h}$ while the input power and other inputs remain constant. It can be seen from the table that when $ZT_{\infty h}$ equals to 2.0, the COP of the optimum air-to-liquid TEAC design yields a value of about 2.6. This value makes the TEAC very comparable with the commercial compressor-based air-conditioners since the latter one has an approximate COP of 2.5.

Table 6.4.

Air-to-liquid Optimum Design for Different ZT Values [35]

$ZT_{\infty h}$ = 0.756 (Present)	$ZT_{\infty h}$ = 1.0	$ZT_{\infty h}$ = 1.3	$ZT_{\infty h}$ = 2.0
$T_c = 16.79\ ^oC$	$T_c = 15.88\ ^oC$	$T_c = 14.96\ ^oC$	$T_c = 13.44\ ^oC$
$T_h = 35.35\ ^oC$	$T_h = 35.95\ ^oC$	$T_h = 36.26\ ^oC$	$T_h = 36.87\ ^oC$
$G_{e,opt.} = 0.93$ cm	$G_{e,opt.} = 0.84$ cm	$G_{e,opt.} = 0.75$cm	$G_{e,opt.} = 0.61$ cm
$I_{opt.} = 13.66$ A	$I_{opt.} = 14.54$ A	$I_{opt.} = 15.32$ A	$I_{opt.} = 16.54$ A
$P_{in} = 401.22$ W	$P_{in} = 399.26$ W	$P_{in} = 398.86$ W	$P_{in} = 400.53$ W
$COP_{opt.} = 1.68$	$COP_{opt.} = 1.87$	$COP_{opt.} = 2.25$	$COP_{opt.} = 2.61$
$Q_c = 672.38$ W	$Q_c = 746.83$ W	$Q_c = 896.20$ W	$Q_c = 1046$ W
$PD_{opt.} = 0.934$ W/cm^2	$PD_{opt.} = 1.037$ W/cm^2	$PD_{opt.} = 1.25$ W/cm^2	$PD_{opt.} = 1.45$ W/cm^2
Inputs: $T_{\infty c} = 23.55\ ^oC$, $T_{\infty h} = 31.09\ ^oC$, $L = 120$mm, $W = 300$mm, $A_b = 720$ cm^2, $H = 50$mm, $n = 880$, $b_c = 15$mm x 2, $b_h = 5$mm, $V_c = 60$ CFM, $V_h = 7$ L/min, $h_c = 35.78$ W/m^{2}K, $h_h = 2922$ W/m^{2}K, $\eta_c h_c A_c = 1.28$ W/K, $\eta_h h_h A_h = 3.07$ W/K, $N_h = 0.417$			

6.3 Air-to-air TEAC Study

In this section, the air-to-air optimum design is modeled based on the inputs found in section 6.2 (same base area, cold air flow rate, and input power), but with a larger height. The total height of the air-to-air TEAC has to be increased so that the results can match the DOE required performance (COP of 1.3 at input power of 400W). Also, when air is used instead of liquid at the hot side, a larger area is needed to release the heat. Therefore, the air-to-air TEAC is modeled based on two layers of thermoelectric modules attached to two heat sinks for the hot air while one heat sink for the cold air is sandwiched between the cold sides of the thermoelectric modules as shown in Figure 4.1. The modeling procedure is similar to the air-to-liquid TEAC where a unit cell is defined at the center of the system.

6.3.1 Optimizing the Heat Sink Parameters

This section shows the results of the concepts discussed earlier on optimizing the heat sink parameters. The goal is to have the minimum possible thermal resistance for both cold and hot heat sinks (or maximizing $\eta_c h_c A_c$ and $\eta_h h_h A_h$). At a given base area ($A_b = 30 \times 30mm^2$) and a profile length ($20mm$ for cold heat sink and $25mm$ for hot heat sink), the fin spacing and thickness are both optimized to give the maximum possible rate of heat transfer. After using equation 2.85 to calculate the optimum fin spacing, the fin thickness can be optimized for maximum heat transfer by using equation 2.86. Figure 6.5 shows the results of heat transfer vs. fin thickness for (a) cold side heat sink and (b) hot side heat sink.

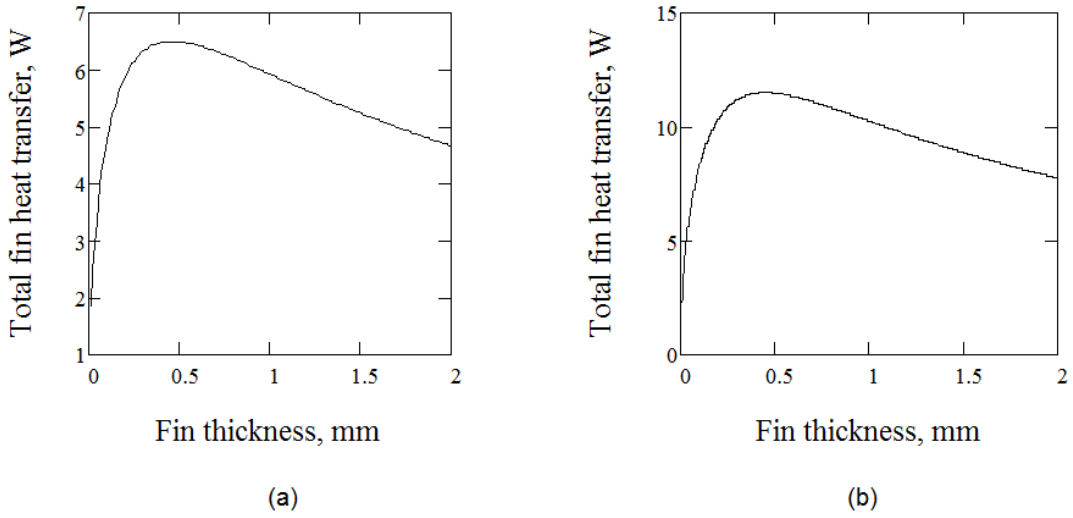

Figure 6.5. Unit cell total heat transfer from heat sink vs. fin thickness for (a) cold side heat sink, (b) hot side heat sink.

6.3.2 Optimum Design of the Unit Cell of Air-to-air TEAC

A schematic of one unit cell is shown in Figure 6.6, where the unit cell cold fluid temperature, $T_{\infty c}$, and hot fluid temperature, $T_{\infty h}$, are averaged based on Gentherm input

parameters. After that, the optimum non-dimensional method can be applied to give the maximum possible COP at a given input power.

Table 6.5 shows the results of the air-to-air TEAC optimum design and compares them with the air-to-liquid TEAC prediction and air-to-liquid TEAC optimum design. Doubling the total height of the air-to-air TEAC, while the base area is maintained similar to the air-to-liquid system, one can calculate the ability of the air-to-air TEAC design to reach the DOE requirement.

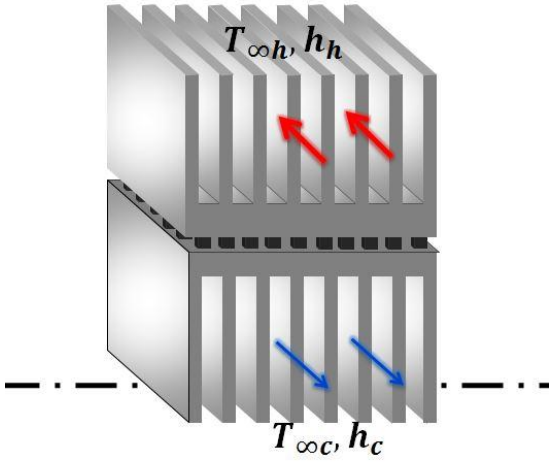

Figure 6.6. Unit cell schematic of air-to-air TEAC [35]

Table 6.5

Results of Air-to-Air Optimum Design Compared with Air-to-Liquid Prediction and Air-to-Liquid Optimum Design [35]

Parameters	**Air-to-air Opt. Design**	**Air-to-liquid Prediction (Gentherm base)**	**Air-to-liquid Opt. Design**
$P_{in}\ (W)$	400.02	409.59	401.22
COP	1.3	1.3	1.68
$Q_c\ (W)$	519.85	533.02	672.38
$PD\ (W/cm^2)$	0.722	0.74	0.934
$W\ (mm) \times L\ (mm)$	300×120	300×120	300×120
$H\ (mm)$	100	50	50

Air-to-air Opt. Design Parameters:
$T_{\infty c,in} = 30.0°C,\ T_{\infty h,in} = 30.0\ °C,\ \Delta T_{cooling} = 16.8\ °C,\ A_b = 720\ cm^2,\ A_{UC} = 30\ mm \times 30\ mm,\ b_c = 50\ mm$, $t_c = 0.46$ mm, $t_h = 0.45$ mm, $z_c = 1.54$ mm, $z_h = 1.0$ mm, $b_h = 25\ mm \times 2$, $V_c = 60$ CFM, $V_h = 140$ CFM, $Re_c = 460.0,\ Re_h = 730.5$, $Nu_c = 7.29$, $Nu_h = 7.6$, $h_c = 65.5 \frac{W}{m^2K}, h_h = 107.2 \frac{W}{m^2K}$, $N_h = 0.51$, $ZT_{\infty h} = 0.763,\ n_{opt.} = 6569, G_e = 0.08cm, I_{opt.} = 1.3\ A$,

6.4 Unit Cell Experimental Validation

The results from the unit cell experimental setup that were discussed in section 5.1 are addressed in this section. First, the junction temperatures are compared in order to study the accuracy of the analytical model. This comparison has been made at given cold and hot ambient temperatures, electrical current, and air flow rates. The analytical junction temperatures are obtained by using the basic heat balance equations (equations 4.5 to 4.8) where the effective material properties are applied. On the other hand, the experimental junction temperatures are obtained by extrapolating the temperature readings from the aluminum blocks as discussed earlier. Figure 6.7 presents the comparison between the analytical and experimental thermoelectric junction temperatures for all three tested TE modules and it shows a very good agreement. Furthermore,

another comparison is addressed to show the performance of the three tested modules as shown in Figure 6.8. This figure also shows a good agreement between experimental and analytical COP vs. input power for all the three tested modules.

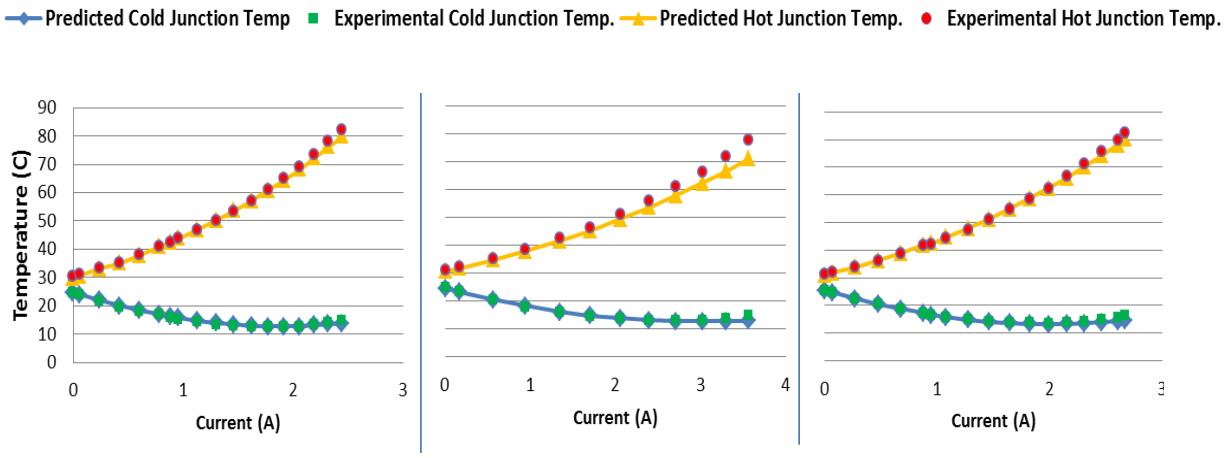

(a) (b) (c)

Figure 6.7. Comparison between experimental and analytical junction temperatures vs. input current for (a) module 1, (b) module 2, and (c) module 3. [36]

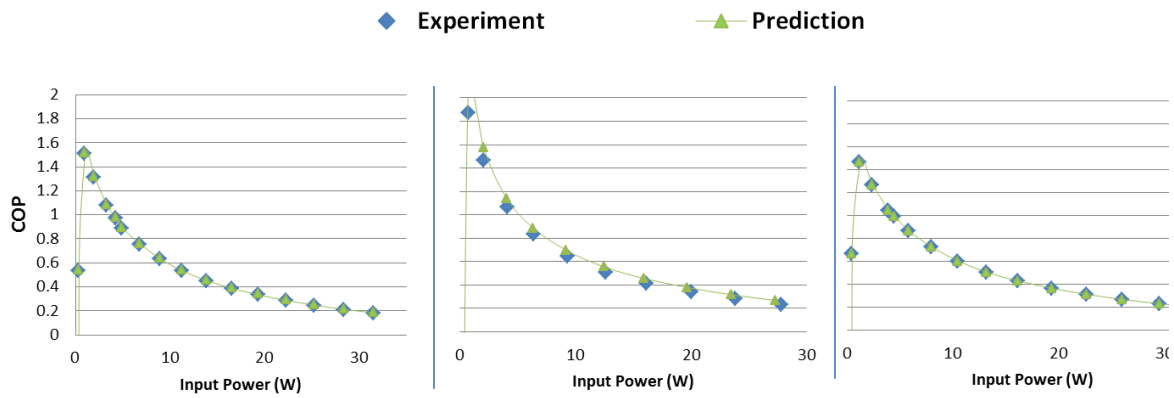

(a) (b) (c)

Figure 6.8. Comparison between experimental and analytical COP vs. input power for (a) module 1, (b) module 2, and (c) module 3. [36]

The optimum design model was designed to find the maximum possible COP at a given input power by optimizing the dimensionless current, N_I, and the ratio of thermal conductance to the convection conductance, N_k. The input power of the whole TEAC system is 360W, which makes the input power of the unit cell to be equal to 4.5W.

Table 6.6 shows the comparison between the three tested modules where different values of N_k is represented by different sizes of TEC modules. The table also shows the optimized results when the aluminum blocks are removed and when the optimum heat sinks are used. It can be seen that the aluminum blocks act negatively on the TEAC performance but using the commercial heat sinks instead of the optimized one has a greater impact.

Table 6.6

Comparison Between the Three Tested Modules, Optimized Design Without the Aluminum Blocks, and the Optimum Design Using the Optimized Heat Sink. [36]

Module	N_I	I **(Amp)**	N_k	$n \times G_e$ (cm)	P_{in} **(W)**	**COP**
1	0.162	0.92	0.258	9.22	4.5	1.044
2	0.199	1.42	0.18	7.08	4.5	1.085
3	0.155	0.96	0.28	11.42	4.5	1.025
Analytical model	0.204	1.46	0.172	6.77	4.5	1.09
w/o blocks	0.219	2.9	0.154	11.21	4.5	1.16
w/o blocks & w/ optimal heat sinks	0.189	2.98	0.119	17.94	4.5	1.38

One of the goals of the experiment is to investigate the effect of the element geometric ratio (or thermoelectric number of couples) at the optimum input electrical current. This goal can be addressed by analyzing the ratio of thermal conductance to the convection conductance, N_k, and its relationship with the optimized design. Testing three different modules validates that goal and shows closest module to the optimum design. Figure 6.9 shows a prediction and comparison of COP vs. N_k between the three modules when the input power is fixed at 4.5W. The predicted curve can be generated by fixing the input power and assuming a constant temperature difference at the junctions (for a short range) and then resolved for N_I to be only as a function of N_k. This assumption allows expressing COP to be independent of N_I for that range where the three tested modules can be included. The figure shows that module 2 has the highest COP and is

considered to be the best module among three at the given conditions due to its closest values of N_k and N_I to the analytical optimal design.

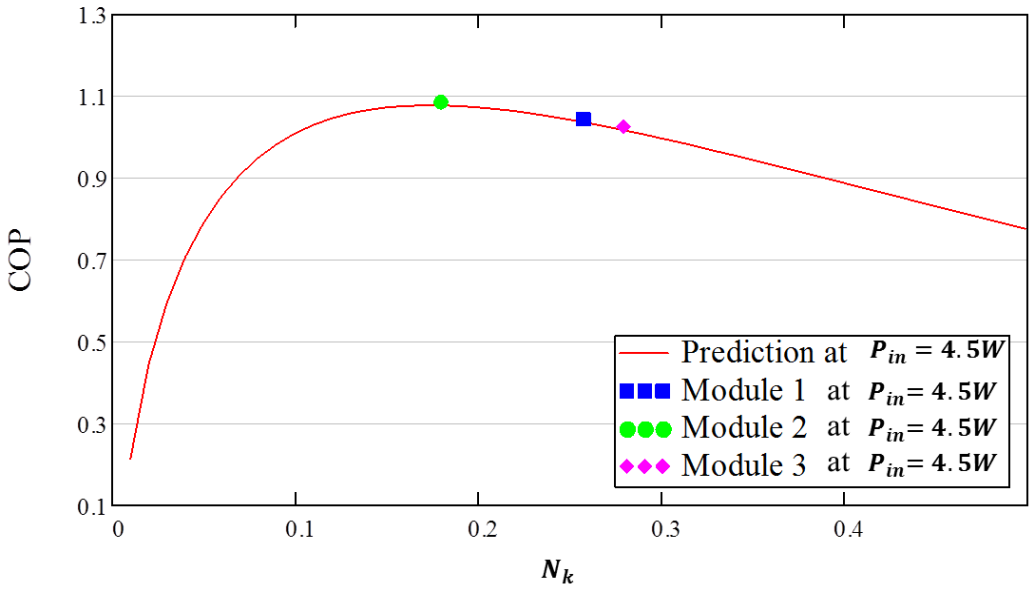

Figure 6.9. COP vs. Nk at Pin = 4.5W. [36]

6.5 Results of the Whole TEAC System

This section discusses the results of the optimum design of the whole air-to-air TEAC modeling that was shown in section 4.3 and its experimental validation. The results are approached by combining the dimensionless method and the thermal isolation method and then comparing these results with an experiment built for that purpose as it was discussed in 5.2. The inputs for this design are: input of electrical power, inlet cold ambient temperature, inlet hot ambient temperature, cold air flow rate, and hot air flow rate and they are equal to 20W, 30^{o}C, 30^{o}C, 3CFM, and 6CFM, respectively. Using the modified dimensionless equations (equations 4.33 to 4.36), a simultaneous prediction of the optimum current and number of thermocouples can be obtained in order to maximize

the COP at a given input power. Figure 6.10 shows COP, cooling power, and input power vs. (a) dimensionless electrical current, N_I, and (b) the ratio of thermal conductance to the convection conductance, N_k, for all of the four units. It can be pointed out from the figure that when the input power is 20W, a higher COP can be obtained if each TEC module maintains its input power to be around 5W.

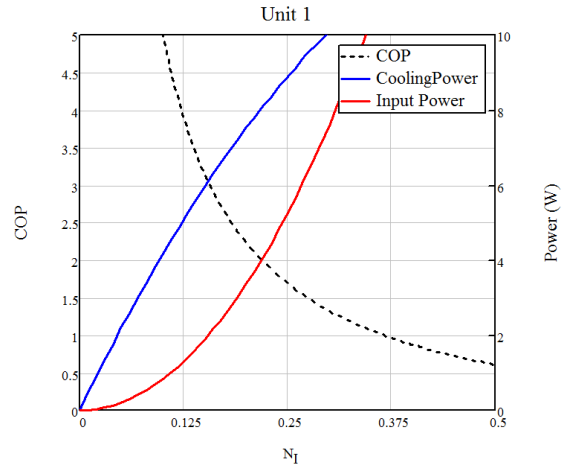

(a)

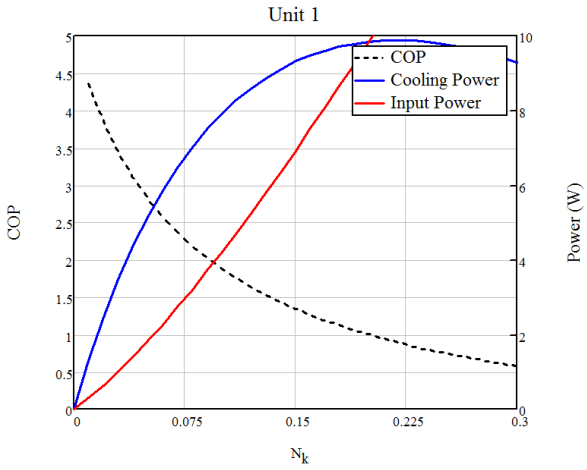

(b)

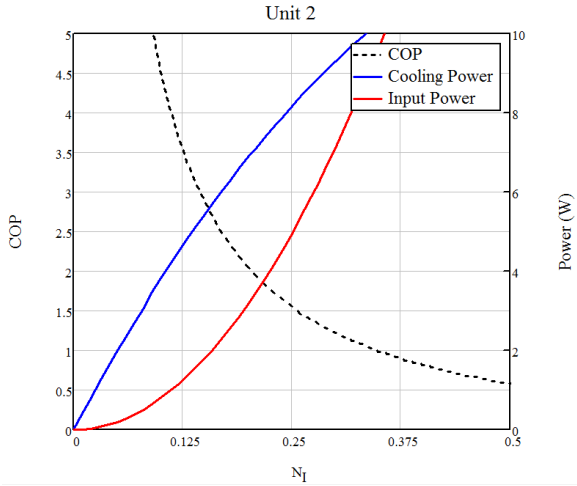

(c)

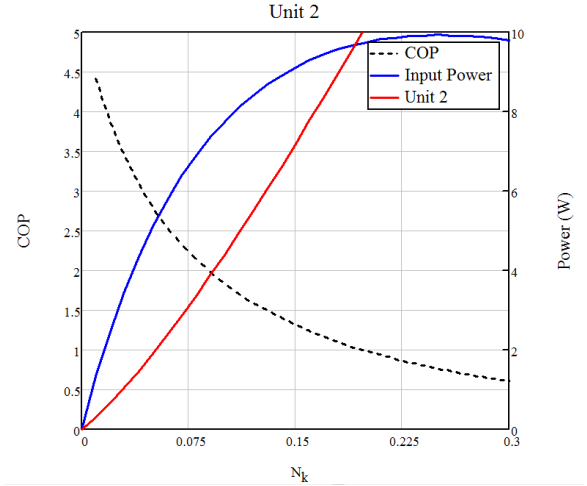

(d)

Figure 6.10—Continued

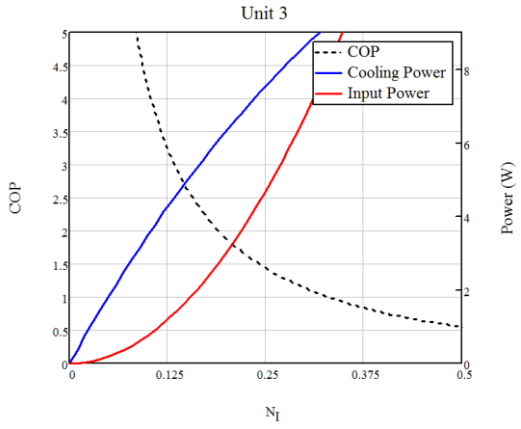

(e)

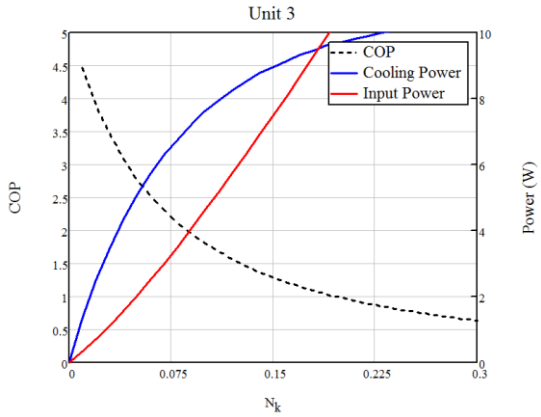

(f)

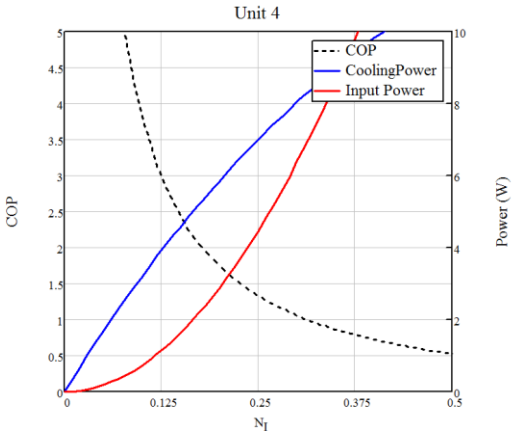

(g)

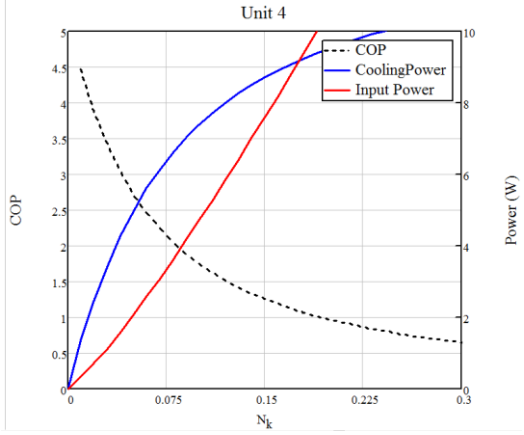

(h)

Figure 6.10. COP, cooling power, and input power vs. dimensionless electrical current, $\boldsymbol{N_I}$, and the ratio of thermal conductance to the convection conductance, $\boldsymbol{N_k}$, for unit 1 (a, b), 2 (c, d), 3 (e, f), and 4 (g, h).

In order to compare and study the accuracy of the analytical model with the experiment, another modified analytical model is built based on the experimental

parameters. The results of the new model can be compared with the experiment as shown in Figure 6.11 (a) and (b) where the cold and hot junction temperatures of the experiment and analytical model are generated against the electrical current. The modified analytical model is built based on the six basic ideal equations (Eqs. 4.33 to 4.36) where the thermal resistance of the aluminum block is considered along with the dimensions of the commercial heat sinks and TEC modules. Solving these equations allow us to obtain the cold and hot junction temperatures which can be compared with the experimental junction temperatures that are obtained by extrapolating the temperature readings from the aluminum. Generally, the results from the figure show very good agreement between the analytical model and the experimental model. However, at a higher current, the error increases especially for the unit cell number 1 and 2. A possible justification for that is due to the use of the effective material properties which are temperature independent properties and were obtained around room temperature; while the actual thermoelectric material properties depend on the temperature and may have different values at higher temperatures. Since the errors only appear at two unit cells and at a higher current, the consideration of these errors may not greatly affect the performance of the whole TEAC system.

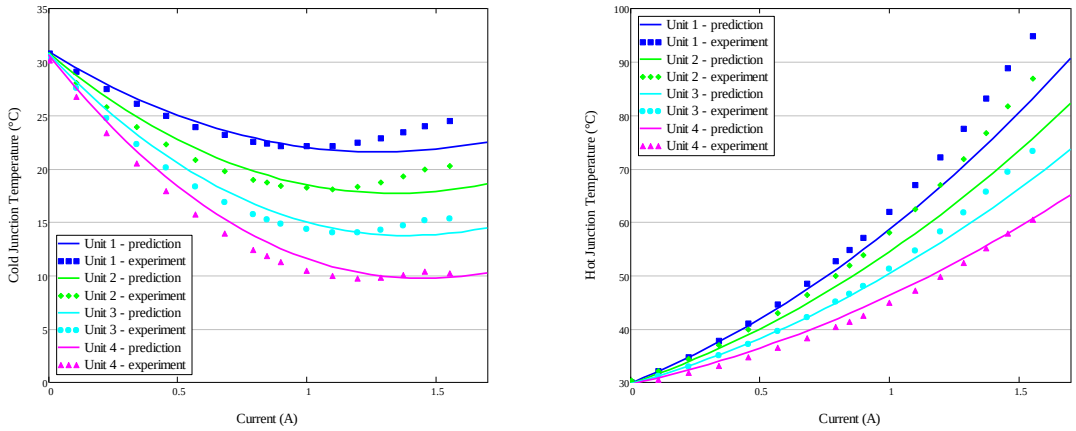

(a) (b)

Figure 6.11. Comparison between experiment and predicted junction temperatures vs. input current for (a) cold junction temperature and (b) hot junction temperature. [37]

Furthermore, the performance of the analytical results of the TEAC can be compared with the experimental performances as shown in Figure 6.12. The figure shows the COP on one side and the difference between ambient and exit cold air temperatures on the other side vs. the input power for both analytical model and experiment. It can be concluded from the figure that the basic heat balance equations with the effective material properties predict the TEAC performance very well. Moreover, the figure shows the improvement of the performance when removing the aluminum blocks and using the optimized heat sinks. In addition to the figure, Table 6.7 compares the experiment, the prediction, and the optimum design using the optimized heat sinks and without the aluminum blocks at input power of 400W. The table also shows that the optimum design has lower thermal resistances (for cold and hot side) and different electrical current and number of thermocouples from the tested system.

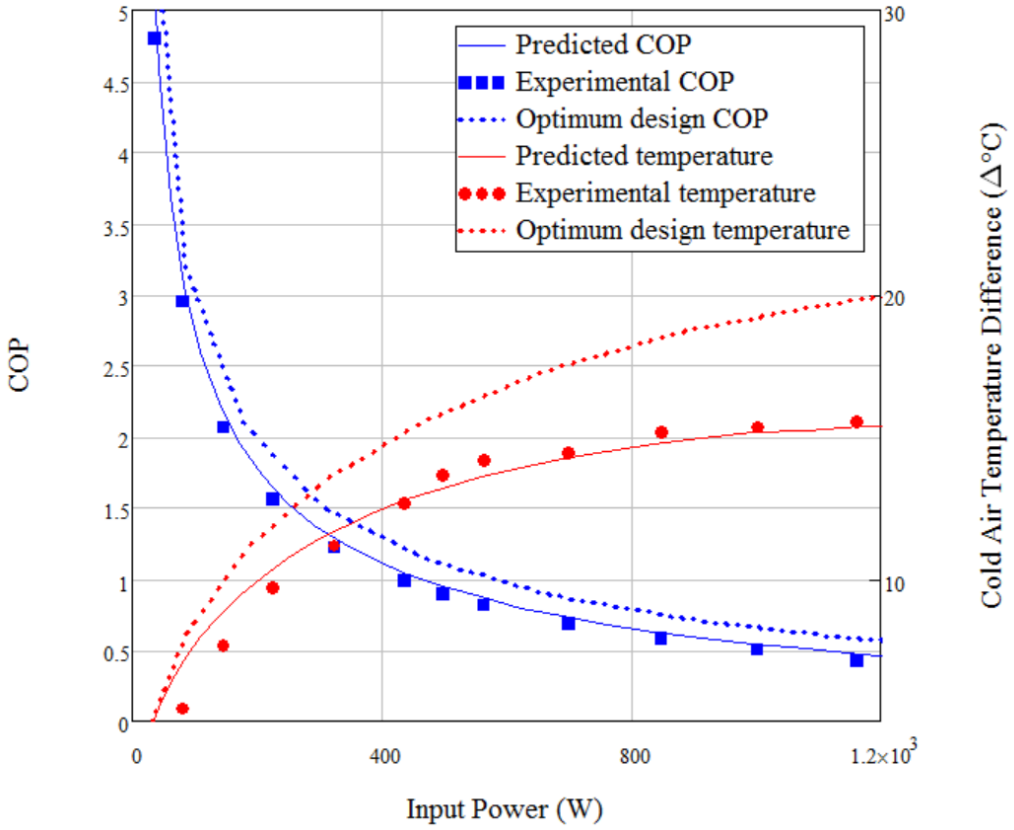

Figure 6.12. Comparison between experiment and predicted COP and cold air temperature difference vs. input power. [37]

Table 6.7

Comparison of the Results between the Experiment, Prediction, and Optimum Design. [37]

	R_c (K/W)	R_h (K/W)	N_I	I_m (A)	N_k	n_{total}	$\dot{Q}_{c,total}$ (W)	COP_{total}
Experiment	0.996	0.848	0.257	0.755	0.131	508	419.85	1.06
Prediction	0.996	0.848	0.257	0.761	0.131	508	444.47	1.11
W/o blocks and with optimal heat sinks	0.867	0.484	0.194	0.57	0.127	862	506.54	1.27

Given: $T_{\infty c,in} = 30^oC$, $T_{\infty h,in} = 30^oC$, $\dot{V}_{c,total} = 60CFM$, $\dot{V}_{h,total} = 120CFM$, $P_{in,total} = 400W$, $G_e = 0.04cm$, and $ZT_{\infty h,in} = 0.804$

CHAPTER 7

CONCLUSION

This current work was focused on the optimization of a counter flow air-to-air TEAC system. The goal was reached by utilizing an optimal design theory and dimensional analysis technique, which allowed for the optimization of the thermoelectric parameters simultaneously. First, this method was applied on a unit cell located at the center of the TEAC system, which allowed study of the optimum design and its feasibility. Further studies were conducted in order to simulate the optimum design of a whole TEAC system from given inlet parameters (i.e., hot and cold air mass flow rates and ambient temperatures). The model was built by combining the optimal design method and the thermal isolation method so that the thermoelectric parameters of the whole system could be optimized. Based on the designed models, two experiments (for the unit cell and the whole TEAC system) were conducted in order to study the accuracy of the analytical models. Although the analytical model was built based on thermoelectric ideal equations, the results showed good agreements with the experiments. These agreements were mainly due to the use of the thermoelectric effective material properties. The validation of the analytical model provides an uncomplicated method to study the optimum design at given inputs.

At the present time, thermoelectric applications are still limited due to their lower efficiency and performance, which is caused from a lower figure of merit. The figure of

merit improvement is a technology-dependent work with numerous amounts of research and signs of development. Recently, a record was registered to have a figure of merit of 2.6 [40], which brings the hope that thermoelectric applications in automotive air conditioning systems are closer than expected.

While higher figures of merit are promising, this by itself is not enough for practical thermoelectric applications. Proper thermal design and optimization of the whole thermoelectric system is also another important area with a lot left to discover. Attending four of the International Conferences on Thermoelectrics (ICT) and having discussions with pioneers in the field leads the researcher to believe that optimizing thermoelectric system is very challenging work due to the number of parameters related to each other. Many institutions use costly experiments or time-consuming finite element simulations to optimize their designs. The analytical techniques used in this work could add simplified bases of the optimization concepts, and hopefully contribute to an optimistic future for thermoelectric applications. These techniques can also be modified and applied in other thermoelectric applications, including thermoelectric power generation, which is also another hope for generating green power.

REFERENCES

[1] D. Crane and G. Jackson, "Optimization of cross flow heat exchangers for thermoelectric waste heat recovery," *Energy Conversion and Management*, vol. 45, no. 9-10, pp. 1565-1582, 2003.

[2] H. Lee, Thermal Design: Heat Sinks, Thermoelectrics, Heat Pipes, Compact Heat Exchangers, and Solar Cells, Hoboken: John Wiley & Sons, Inc., 2010.

[3] J. R. Sootsman, D. Y. Chung and M. G. Kanatzidis, "New and Old Concepts in Thermoelectric Materials," *Angewandte Chemie International Edition*, vol. 48, no. 46, p. 24, 2009.

[4] J. R. Sootsman, D. Y. Chung and M. G. Kanatzidis, "Thermoelectrics: new and old concepts in thermoelectric materials," *Angewandte Chemie International Edition*, vol. 48, no. 46, pp. 8616-8639, 2009.

[5] C. B. Vining, "An inconvenient truth about thermoelectrics," *Nature Materials*, vol. 8, no. 2, pp. 83-85, 2009.

[6] J. Fairbanks, "Vehicular thermoelectric applications session DEER 2009," U.S. Department of Energy, 05 08 2009. [Online]. Available: http://www1.eere.energy.gov/vehiclesandfuels/pdfs/deer_2009/session7/deer09_fairbanks.pdf. [Accessed 06 11 2013].

[7] C. W. Maranville, "Thermoelectric HVAC and thermal comfort enablers for light-duty vehicle applications," United States Department of Energy, 18 05 2012. [Online]. Available: http://www1.eere.energy.gov/vehiclesandfuels/pdfs/merit_review_2012/adv_combustion/ace047_maranville_2012_o.pdf. [Accessed 06 11 2013].

[8] M. Schlesinger, Modern Electroplating 4TH Edition, Canada: John Wiley & Sons Inc., 2000.

[9] C. W. Maranville, J. Schneider, L. Chaney, T. Barnh and J. P. Heremans, "Improving efficiency of a vehicle HVAC system with comfort modeling, zonal design, and thermoelectric devices," United States Department of Energy, 18 10 2012. [Online]. Available: http://www1.eere.energy.gov/vehiclesandfuels/pdfs/deer_2012/thursday/presentations/deer12_maranville.pdf. [Accessed 06 11 2013].

[10] H. Lee, "Optimal design of thermoelectric devices with dimensional analysis," *Applied Energy*, vol. 106, pp. 79-88, 2013.

[11] L. E. Bell, "Use of thermal isolation to improve thermoelectric system operating efficiency," *IEEE*, no. 21st International Conference on Thermoelectronics (2002), 2002.

[12] H. Lee, A. Attar and S. Weera, "Performance prediction of commercial thermoelectric cooler modules using the effective material properties," *Journal of Electronic Materials*, vol. 44, no. 6, pp. 2157-2165, 2015.

[13] H. Lee, "Manual for thermoelectric coolers," [Online]. Available: http://homepages.wmich.edu/~leehs/ME539/ME539.html. [Accessed 05 11 2015].

[14] K.-i. Uemura, "History of thermoelectricity development in Japan," *Journal of Thermoelectricity*, no. 3, 2002.

[15] J. Koehle, N. C. Lemke, N. C. Strupp and C. S. Junior, "Modeling a thermoelectric HVAC system for automobiles," *Journal of Electronic Materials*, vol. 38, no. 7, pp. 1093-1097, 2009.

[16] J. LaGrandeur, D. Crane and D. Wang, "Design and analysis of a thermoelectric HVAC system for passenger vehicles," *SAE International*, Vols. 2010-01-0807, 2010.

[17] M. S. Raut and D. V. Walke, "Thermoelectric air cooling for cars," *International Journal of Engineering Science and Technology (IJEST)*, vol. 4, no. 5, pp. 2381-2394, 2012.

[18] C.-Y. Hsu, S.-L. Li, C.-K. Liu, R.-M. Tain, H.-C. Chien, S.-F. Hsu, C.-M. Tzeng, M.-J. Dai, H.-S. Chu and J.-D. Hwang, "Non-refrigerant thermoelectric air conditioning technique on vehicles," in *Microsystems, Packaging, Assembly and Circuits Technology Conference (IMPACT), 2011 6th International*, Taipei, 2011.

[19] G. Roumayah, D. Thomas and T. Barnhart, "Development of a thermoelectric device for an automotive zonal HVAC system," United States Department of Energy, 20 03 2011. [Online]. Available: https://www1.eere.energy.gov/vehiclesandfuels/pdfs/thermoelectrics_app_2012/tuesday/barnhart.pdf. [Accessed 06 11 2013].

[20] W. Chen, C. Hung and C. Wang, "Design of heat sink for improving the performance of thermoelectric generator using two-stage optimization," *Energy*, vol. 39, no. 1, pp. 236-245, 2012.

[21] M. H. M. Makhmalbaf, "Experimental study on convective heat transfer coefficient around a vertical hexagonal rod bundle," *Heat Mass Transfer*, vol. 48, pp. 1023-1029, 2012.

[22] P. Teertstra, M. Yovanovich, J. Culham and T. Lemczyk, "Analytical forced convection modeling of plate fin heat sinks," in *Semiconductor Thermal Measurement and Management Symposium*, San Diego, CA, USA, 1999.

[23] W. Zhimin and C. K. Fah, "The optimum thermal design of microchannel heat sinks," in *Electronic Packaging Technology Conference*, 1997.

[24] M. Yamanashi, "A new approach to optimum design in thermoelectric cooling systems," *Journal of Applied Physics,* vol. 80, no. 9, pp. 5494-5502, 1996.

[25] X. C. Xuan, "Optimum design of a thermoelectric device," *Semiconductor Science and Technology,* vol. 17, no. 2, pp. 114-119, 2002.

[26] J. Chen, B. Lina and Y. Pan, "Performance analysis and parametric optimal design of an irreversible multi-couple thermoelectric refrigerator under various operating conditions," *Applied Energy,* vol. 84, no. 9, pp. 992-892, 2007.

[27] C.-T. Hsu, G.-Y. Huang, H.-S. Chu, B. Yu and D.-J. Yao, "Experiments and simulations on low-temperature waste heat harvesting system by thermoelectric power generators," *Applied Energy*, vol. 88, no. 4, pp. 1291-1297, 2011.

[28] M. A. Karri, E. F. Thacher and B. T. Helenbrook, "Exhaust energy conversion by thermoelectric generator: Two case studies," *Energy Conversion and Management,* vol. 52, no. 3, pp. 1596-1611, 2011.

[29] D. M. Rowe, Thermoelectrics Handbook: Micro to Nano, New York: Taylor &, 2006.

[30] L. Chen , J. Gong, F. Sun and C. Wu, "Effect of heat transfer on the performance of thermoelectric generators," *International Jouranl of Thermal Sciences,* vol. 41, pp. 95-99, 2002.

[31] X. Gou, H. Xiao and S. Yang, "Modeling, experimental study and optimization on low-temperature waste heat thermoelectric generator system," *Applied Energy,* vol. 87, pp. 3131-3136, 2010.

[32] G. Casano and S. Piva, "Experimental investigation of the performance of a thermoelectric generator based on Peltier cells," *Experimental Thermal and Fluid Science,* vol. 35, pp. 660-669, 2011.

[33] Y.-W. Chang, C.-C. Chan, M.-T. Ke and S.-L. Chen, "Thermoelectric air-cooling module for electronic devices," *Applied Thermal Engineering*, vol. 29, pp. 2731-2737, 2009.

[34] H.-S. Huang, Y.-C. Weng, Y.-W. Chang, S.-L. Chen and M.-T. Ke, "Thermoelectric water-cooling device applied to electronic equipment," *International Communications in Heat and*

Mass Transfer, vol. 37, pp. 140-146, 2010.

[35] A. Attar, H. Lee and S. Weera, "Optimal design of automotive thermoelectric air conditioner (TEAC)," *Journal of Electronic Materials*, vol. 43, no. 6, pp. 2179-2187, 2014.

[36] A. Attar, H. Lee and S. Weera, "Experimental validation of the optimum design of an automotive air-to-air thermoelectric air conditioner (TEAC)," *Journal of Electronic Materials*, vol. 44, no. 6, pp. 2177-2185, 2015.

[37] A. Attar and H. Lee, "Designing and testing the optimum design of automotive air-to-air thermoelectric air conditioner (TEAC) system," *Energy Conversion and Management*, no. Manuscript sumbitted for publication, 2015.

[38] L. Technology, Thermoelectric Handbook, Laird Technology, [Online]. Available: www.lairdtech.com. [Accessed 07 11 2013].

[39] L. Technology, "Ceramic plate series CP10,127,05 thermoelectric modules," Laird Technology, [Online]. Available: www.lairdtech.com. [Accessed 07 11 2013].

[40] L.-D. Zhao, S.-H. Lo, Y. Zhang, H. Sun, G. Tan, C. Uher, W. C. , D. Vinayak P. and M. G. Kanatzidis, "Ultralow thermal conductivity and high thermoelectric figure of merit in SnSe crystals," *Nature*, vol. 508, no. 7496, pp. 373-377, 2014.